Light scattering from spin waves in thin films and layered systems

1994 J. Phys.: Condens. Matter 6 7145

(http://iopscience.iop.org/0953-8984/6/36/002)

J. Phys.: Condens. Matter 6 (1994) 7145–7188. Printed in the UK

REVIEW ARTICLE

Light scattering from spin waves in thin films and layered systems

S Demokritov and E Tsymbal
Forschungszentrum Jülich, Jülich, Germany

Received 24 January 1994

Abstract. Brillouin light scattering (BLS) is now established as a powerful tool for the investigation of spin waves in layered magnetic structures. Due to the strong magneto-optical interaction in the majority of magnetic metals BLS allows the examination of spin waves in films with extremely small thicknesses down to 1–2 monolayers. This gives us the opportunity to obtain important information about magnetic properties of such two-dimensional systems. Applied to magnetic bilayers and multilayers, BLS makes it possible to elucidate collective excitations in these complex structures as well as to analyse mechanisms of the interlayer coupling. The restricted geometry of layered systems considerably influences the interaction of spin waves with light resulting in many peculiar features of the light-scattering phenomenon.

1. Introduction

An extraordinarily high quality of thin magnetic films and layered systems is a great achievement of the last decade. By growth techniques such as molecular beam epitaxy (MBE), one may create films representing nearly perfect crystals and layered structures with interfaces nearly perfect on atomic scale. Film thicknesses may reach a few or even one atomic layer. It is natural, that such a high quality of the new magnetic systems results in unique static magnetic properties. The dynamic characteristics, namely spin-wave excitations, also possess a number of new features. They are of considerable interest for the understanding of the fundamental magnetic phenomena, like magnetic order in two dimensions. Besides, they depend on static magnetic properties and, therefore, contain valuable information about intrinsic magnetism of layered structures.

There are basically two types of magnetic excitations, which are important in thin films and layered systems. The first one is the so-called surface mode which is determined mainly by dipolar interaction and does not depend on exchange. It forms near the surface and propagates along the surface. In layered structures the surface modes exist in each magnetic layer, they can be coupled via dipolar stray fields, forming collective magnetostatic spin-wave excitations. The second one is the so-called bulk or standing mode. In thin-film structures the bulk modes are determined dominantly by the magnetic exchange interaction and their wavevector strongly depends on the layer thickness.

Essentially there are three experimental methods to detect spin waves, namely, inelastic neutron scattering, ferromagnetic resonance (FMR) and Brillouin light scattering (BLS). Neutron scattering has its main advantage in the large accessible wavevector range, but, generally, its sensitivity is too low for the application to thin films. FMR is a well developed method in this field. Many of the basic properties of spin waves and magnetic coupling mechanisms have been studied by FMR. However, apart from situations where wavevectors

0953-8984/94/367145+44$19.50

of spin waves are determined by the sample geometry (for example standing modes of thin films) FMR is restricted to zero-wavevector spin excitations. This has an important effect on the types of mode seen by FMR: they do not display dipolar coupling in layered structures.

The BLS technique offers a convenient experimental tool to study non-zero-wavevector spin excitations in magnetic materials. This method is based on the process of inelastic light scattering from spin waves. The essence of this process can be understood as follows. Spin waves in magnetic material cause a spatially periodic modulation of the permittivity of the medium. Interaction of incident light with the permittivity fluctuations leads to light scattering. The inelastic light-scattering process involves a magnetic excitation (one-magnon process): in a Stokes scattering process the spin wave is created; in an anti-Stokes process the spin wave is destroyed. The two-magnon processes in which two spin waves are created or destroyed are also possible. The intensity of the scattered light is proportional to the magneto-optic coupling (see section 3). Therefore, the BLS method turns out to be particularly useful in the case of metallic films and magnetic semiconductors because of their strong magneto-optic interaction.

The wavevector of detected spin waves k is determined by the momentum transfer from incident light to spin waves in the inelastic light scattering process. For the one-magnon BLS the available range of k is of the order of 10^3–10^6 cm^{-1}. It is determined by the wavelength of incident light ($\sim 10^{-5}$ cm) as well as the geometry of the experiment. The peculiar feature of this region of wavevectors is that the magnetic, dipolar and exchange contributions to the spin-wave energy are comparable. Therefore, changing k and external magnetic field one can study the principally different mechanisms of the formation of spin waves.

BLS has another advantage in that the probe wavelength (i.e. the wavelength of light) is generally much smaller than the sample, in contrast to FMR where the opposite is usually true. It is, therefore, possible to probe local regions and surfaces. For instance, in cases where the light penetration depth is small (as for metals), the surface region can be selectively examined. Another example is the study of interlayer coupling in magnetic bilayers (see subsection 6.1). The small probe region and the usage of wedge-type samples provide a simple way to measure the interlayer coupling as a function of the thickness of a spacer.

The frequencies of spin waves are the main quantities determined in a Brillouin light scattering experiment. As we have already mentioned, they are connected with magnetic properties of thin films and layered systems such as the saturation magnetizations, volume and surface (interface) anisotropies, the values of the exchange intra- and interlayer coupling and others. The intensities of BLS lines as functions of the incident and scattered light polarizations, applied magnetic field, temperature and other physical parameters also characterize the magnetic state of the sample. Thus, BLS spectra contain a lot of information about the magnetism of thin films and layered systems as well as about coupling phenomena between magnetic layers.

After the first observation of the surface spin waves by BLS in the ferromagnetic semiconductor EuO [1], many other measurements in thin films and double and multilayer structures have been reported. They demonstrated scattering from localized surface spin waves as well as a modification of the bulk spin-wave characteristics. Many new phenomena related to magnetic properties of thin-film structures have been studied by BLS from spin waves. Nowadays BLS has proved to be an important and informative tool for the exploration of magnetic excitations in these systems. Several comprehensive reviews [2–4] and a book [5] have been devoted to this subject.

The purpose of this review is to describe the present state of BLS investigations of magnetic thin films and layered systems. We restrict ourselves only by the consideration of

the one-magnon inelastic light scattering. The review is organized as follows. In section 2 a theoretical approach to the evaluation of the frequencies of spin waves in thin films and layered systems is outlined. The features of surface and bulk modes are discussed. The influence of interlayer coupling on the spin-wave frequencies in bilayers is demonstrated. In section 3 a mechanism of light scattering from spin waves is described. Peculiarities of Stokes and anti-Stokes scattering processes and the intensity of lines corresponding to surface and bulk modes are discussed. In section 4 experimental methods of thin-film fabrication and light-scattering techniques are presented. In section 5 papers concerning the study of two-dimensional effects in thin films by BLS are reviewed. In section 6 properties of magnetic layered systems studied by BLS are discussed. Of particular importance are the magnetic interlayer coupling effects. In section 7 the features of non–thermal spin waves, i.e. spin waves excited by pumping microwave radiation, are described.

2. Spin waves in thin films and layered systems

For the description of magnetic excitations in thin films and layered systems a quantum-mechanical approach based on the spin Hamiltonian and solving the Heisenberg equation may be utilized (see e.g. [6]). However, in BLS experiments the relevant wavelengths of spin waves λ are large compared with interatomic spacing ($\lambda \sim 10^{-5}$ cm). This long-wavelength nature of the magnetic excitations allows one to apply a macroscopic continuum model (see e.g. [7, 8, 5, 9]). Such a model starts from the Landau–Lifshitz equation of motion of magnetization M:

$$\frac{\mathrm{d}\boldsymbol{M}(\boldsymbol{r},t)}{\mathrm{d}t} = \gamma \boldsymbol{M}(\boldsymbol{r},t) \times \boldsymbol{H}_{\mathrm{eff}}(\boldsymbol{r},t) \tag{1}$$

where γ is the gyromagnetic ratio (equal to $g\mu_{\mathrm{B}}/\hbar$) and $\boldsymbol{H}_{\mathrm{eff}}$ is the total effective magnetic field. In the general case $\boldsymbol{H}_{\mathrm{eff}}$ includes the external applied field $\boldsymbol{H}_0$, a demagnetizing field $\boldsymbol{H}_{\mathrm{dip}}$, an effective exchange field $\boldsymbol{H}_{\mathrm{ex}}$ and an effective anisotropy field $\boldsymbol{H}_{\mathrm{an}}$. The resulting magnetization $\boldsymbol{M}$ and magnetic field $\boldsymbol{H}_{\mathrm{eff}}$ can be each split into a static part and a fluctuating component, $\boldsymbol{m}(\boldsymbol{r},t)$ and $\boldsymbol{h}(\boldsymbol{r},t)$, the time dependence being of the form $\boldsymbol{m}(\boldsymbol{r},t) = \boldsymbol{m}(\boldsymbol{r})\exp(\mathrm{i}\omega t)$, $\boldsymbol{h}(\boldsymbol{r},t) = \boldsymbol{h}(\boldsymbol{r})\exp(\mathrm{i}\omega t)$. At low temperatures ($T \ll T_{\mathrm{C}}$) fluctuating components $|\boldsymbol{m}|$ and $|\boldsymbol{h}|$ can be assumed to be small compared with static ones, which allows for a linearization of the equation of motion (1).

For the subsequent analysis of the linearized equations and finding their solutions a relationship between $\boldsymbol{h}(\boldsymbol{r})$ and $\boldsymbol{m}(\boldsymbol{r})$ is necessary. For the wavevectors accessible by light-scattering experiments and for rather thin films both exchange and dipolar interactions may contribute to the $\boldsymbol{h}(\boldsymbol{r})$. They result in dipolar-exchange spin modes that are considered below. Nevertheless, the dipolar approximation introduced for the finite-slab geometry by Damon and Eschbach [10] is widely used for the description of magnetic excitations.

This approximation corresponds to the 'magnetostatic' case in which the interaction between the fluctuating spins is mainly dipolar and the effect of exchange is negligibly small. The usual approach which is applied for the treatment of this case is deriving the simultaneous solution of linearized equations of motion and the corresponding Maxwell's equations together with the appropriate electromagnetic boundary conditions. However, there exists another approach (see [11, 12] and references therein), which is based on the direct expression for the dipolar field. The spin-wave modes are obtained in this treatment from the solution of integral equations rather than differential ones. One of the advantages of such a method lies in the fact that the boundary conditions are automatically included in

the integral equations. This approach gives, naturally, the same solutions as the traditional model. However, in some cases it allows one to derive transparent analytical expressions for the frequencies of the spin waves rather than to utilize numerical calculations. Below we will outline the main points of this approach.

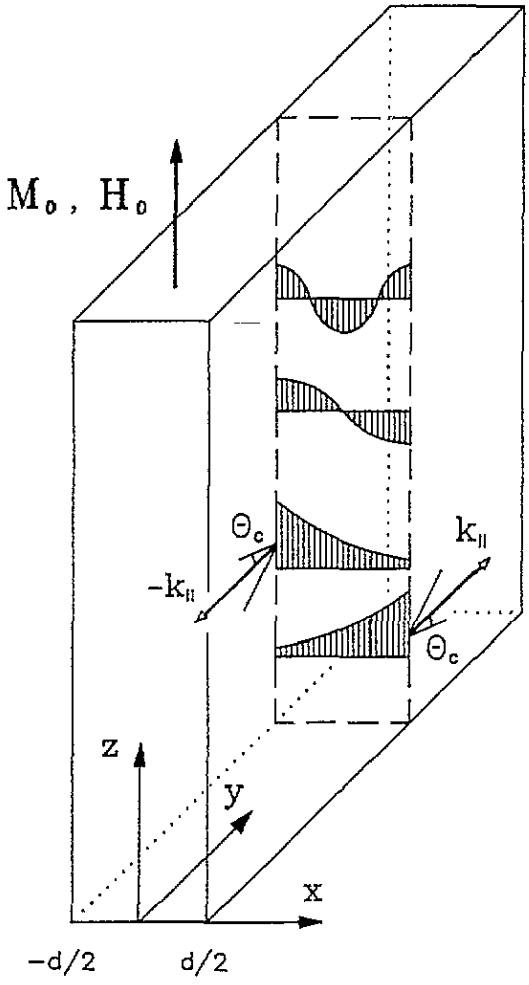

Figure 1. Slab geometry with various types of spin wave indicated. The direction of propagation of the surface modes and the critical angle θ_c are shown. In-plane propagation of the bulk modes is arbitrary.

Let us consider a ferromagnetic slab of thickness d in the x direction (from $x = -d/2$ to $x = d/2$) and infinite in the y and z directions (see figure 1). Let us assume that anisotropy is neglected. Then, if the applied external magnetic field, $\boldsymbol{H}_0$, lies in the z direction, the static magnetization, $\boldsymbol{M}_0$, is also aligned in the z direction. The magnetic dipolar field $\boldsymbol{h}^{\mathrm{dip}}(\boldsymbol{r})$ can be represented as follows:

$$\boldsymbol{h}^{\mathrm{dip}}(\boldsymbol{r}) = -\nabla\Phi(\boldsymbol{r}) \tag{2}$$

where a scalar potential $\Phi(\boldsymbol{r})$ is given by

$$\Phi(\boldsymbol{r}) = \int \frac{\boldsymbol{m}(\boldsymbol{r}')(\boldsymbol{r}-\boldsymbol{r}')}{|\boldsymbol{r}-\boldsymbol{r}'|^3}\,\mathrm{d}\boldsymbol{r}'. \tag{3}$$

Here the integral should be taken over the whole volume of the film. Further, the magnetization $\boldsymbol{m}(\boldsymbol{r})$ and the dipolar field $\boldsymbol{h}^{\mathrm{dip}}(\boldsymbol{r})$ are expanded in terms of two-dimensional Fourier transformation (over y and z) [13]. The resulting equations for the fluctuating part of the magnetization can be written as follows:

$$\begin{aligned} \mathrm{i}\Omega m_x(\boldsymbol{k}_\parallel, x) &= -\frac{1}{4\pi} h_y^{\mathrm{dip}}(\boldsymbol{k}_\parallel, x) + \Omega_H m_y(\boldsymbol{k}_\parallel, x) \\ \mathrm{i}\Omega m_y(\boldsymbol{k}_\parallel, x) &= \frac{1}{4\pi} h_x^{\mathrm{dip}}(\boldsymbol{k}_\parallel, x) - \Omega_H m_x(\boldsymbol{k}_\parallel, x) \end{aligned} \tag{4}$$

where $\Omega = \omega/(4\pi\gamma M_0)$, $\Omega_H = H_0/(4\pi M_0)$, $\mathbf{k}_\parallel$ is the in-plane component of the wavevector of the spin waves and $\boldsymbol{m}(\boldsymbol{k}_\parallel, x)$ and $\boldsymbol{h}^{\mathrm{dip}}(\boldsymbol{k}_\parallel, x)$ are the Fourier components of the magnetization and the dipolar field, respectively. The crucial point is that the dipolar field can be expressed in terms of the magnetization:

$$\boldsymbol{h}^{\mathrm{dip}}(\boldsymbol{k}_\parallel, x) = \int_{-d/2}^{d/2} \mathbf{G}(\boldsymbol{k}_\parallel, x, x')\boldsymbol{M}(k_1 1, x')\mathrm{d}x' \tag{5}$$

where components of the matrix $\mathbf{G}(\boldsymbol{k}_\parallel, x, x')$ are given in [11, 12]. The relation (5) makes it possible to consider (4) as integral equations in respect to the magnetization $\boldsymbol{m}(\boldsymbol{k}_\parallel, x)$. They relate values of the magnetization over the whole thickness of the film including the surface, i.e. the boundary conditions are involved in them.

There are two kinds of solutions of (4) for a finite slab. One of them is

$$\boldsymbol{m}(\boldsymbol{k}_\parallel, x) = \boldsymbol{m}^{(1)}(\boldsymbol{k}_\parallel)\exp(\mathrm{i}k_x x) + \boldsymbol{m}^{(2)}(\boldsymbol{k}_\parallel)\exp(-\mathrm{i}k_x x) \tag{6}$$

where k_x is a real wavevector component along the x direction. It corresponds to a bulk spin wave, which has the dispersion behaviour

$$\Omega^2 = \Omega_{\mathrm{B}}^2(\boldsymbol{k}) = \Omega_H\left[\Omega_H + \left(1 - \frac{k_z^2}{k^2}\right)\right] \tag{7}$$

where $\boldsymbol{k} = \{k_x, k_y, k_z\}$ is the wavevector in the direction of spin-wave propagation. As is seen from (7), frequency $\Omega_{\mathrm{B}}(\boldsymbol{k})$ depends only on the angle θ between $\boldsymbol{k}$ and z axis (the magnetization direction). The manifold of bulk spin-wave states extends from frequency Ω_H, when $k_x = k_y = 0$ ($\theta = 0$), up to frequency $[\Omega_H(\Omega_H + 1)]^{1/2}$, when $k_z = 0$ ($\theta = 90°$). The reason for this anisotropy lies in the anisotropy of the dipolar interaction.

The other type of solution has the form

$$\boldsymbol{m}(\boldsymbol{k}_\parallel, x) = \boldsymbol{m}^{(3)}(\boldsymbol{k}_\parallel)\exp\left[k_0\left(x - \frac{d}{2}\right)\right] + \boldsymbol{m}^{(4)}(\boldsymbol{k}_\parallel)\exp\left[-k_0\left(x + \frac{d}{2}\right)\right] \tag{8}$$

where k_0 is real and positive. This solution is the sum of two terms, each of them having the largest amplitude at the surface but decaying exponentially with distance from the surface.

Therefore, it represents a surface magnetostatic mode. The value of the decay constant k_0 defines the attenuation length k_0^{-1} of the surface spin wave. For transverse propagation, i.e. $k_\parallel = k_y$ ($k_z = 0$), the decay constant k_0 is equal to $k_\parallel$ and the frequency of the surface mode is given by [10]

$$\Omega = \Omega_S(k_\parallel) = \sqrt{(\Omega_H + \tfrac{1}{2})^2 - \tfrac{1}{4}\exp(-2k_\parallel d)}. \tag{9}$$

It is seen from (9) that for large enough d ($k_\parallel d \gg 1$) Ω_S approximates to the value $(\Omega_H + \frac{1}{2})$. If d is decreased the surface wave frequency predicted by (9) decreases and reaches the frequency of the bulk mode $[\Omega_H(\Omega_H + 1)]^{1/2}$ at $\theta = 90°$. The profiles of two bulk modes are shown schematically in figure 1.

As was shown in [10] the surface mode has a peculiar dependence on the direction of propagation. For half-space medium it exists only for propagation along the surface into an angle $\theta \leqslant \theta_c$ around the direction normal to the magnetization. The critical angle θ_c is defined by

$$\tan\theta_c = \sqrt{\Omega_H}. \tag{10}$$

Outside this range of θ there are no surface modes. For transverse propagation ($\theta = 90°$) the attenuation length k_0^{-1} is equal to $k_\parallel^{-1}$. When θ is approaching the critical angle, the attenuation length decreases and vanishes at θ_c. Hence at the critical angle the surface mode is completely localized at the surface. The surface magnetostatic modes of the finite slab have also non-reciprocal propagation properties. If for some direction of $k_\parallel$ there is a surface mode localized near the surface at $x = -d/2$, then for $k_\parallel$ reversed in direction the surface mode is concentrated on the $x = d/2$ surface. The localization increases on approaching the critical angle defined by (10). The two surface modes with opposite directions of $k_\parallel$ are degenerate, i.e. they have the same frequency and the same attenuation length. The profiles of the surface modes as well as their directions of propagation are shown in figure 1. The aforementioned non-reciprocal propagation properties of the surface spin waves are revealed in intensities of the Stokes and anti-Stokes components of BLS spectra that will be discussed in the following section.

The theory allows one to take into account the volume anisotropy. In particular, in the case of volume uniaxial anisotropy, if the external magnetic field and the static magnetization are aligned along the easy axis (z axis), it can be made straightforward. More complicated situations are considered, e.g. in [14].

The problem of determining the character of magnetic excitations in thin films, when both dipolar and exchange interactions are essential, is more complicated. There has been a considerable number of papers addressed to this problem (see e.g. review [8]). The usual approach which is utilized for the analysis of the *dipole-exchange modes* is based on the straightforward solution of the linearized equation of motion together with appropriate boundary conditions. However, even in the simplest case of a single layer without anisotropies (see, for example, [15]) one should apply numerical calculations, which do not always give a clear understanding of the obtained results.

In the majority of cases (especially for rather thin films) the approach to the treatment of the dipole-exchange modes, proposed by Kalinikos and Slavin [11] and developed by Vayhinger and Kronmüller [12] appears to be extremely useful. It is based on the integral expression (5) for the dipolar interaction and allows one to apply the perturbation theory. The latter simplifies drastically numerical calculations and in a number of cases makes it possible to obtain clear analytical results.

To examine the influence of exchange one should include in $\boldsymbol{H}_{\text{eff}}$ in the equation of motion (1) the effective exchange field $\boldsymbol{H}_{\text{ex}}$. For wavelengths which are large compared with the atomic spacing it can be written as follows [7]:

$$\boldsymbol{H}_{\text{ex}}(\boldsymbol{r}, t) = -\frac{2A}{M_0}\nabla^2 \boldsymbol{M}(\boldsymbol{r}, t) \tag{11}$$

where A is the exchange stiffness parameter. Assuming that the magnetization and the effective magnetic field consist of a static part in the z direction and a small fluctuating component in the x–y plane one can obtain in analogy with (4)

$$\begin{aligned}\left(\Omega_H - \alpha\frac{\mathrm{d}^2}{\mathrm{d}x^2} + \alpha k_\parallel^2\right) m_x(x) &= -\mathrm{i}\Omega m_y(x) + \frac{1}{4\pi} h_x^{\text{dip}}(x) \\ \left(\Omega_H - \alpha\frac{\mathrm{d}^2}{\mathrm{d}x^2} + \alpha k_\parallel^2\right) m_y(x) &= \mathrm{i}\Omega m_x(x) + \frac{1}{4\pi} h_y^{\text{dip}}(x)\end{aligned} \tag{12}$$

where $\alpha = (2A)/(4\pi M_0^2)$ and h_x^{dip}, h_y^{dip} are defined by equation (5).

Further, the appropriate boundary conditions have to be imposed at each surface. They were derived by Rado and Weertman [16]. For the case of parallel aligned magnetization the Rado–Weertman boundary conditions can be represented as follows:

$$\begin{aligned}\pm A\frac{\partial m_x}{\partial x}\bigg|_{x=\pm d/2} &= (K_{\text{S}}^{\perp} + K_{\text{S}}^{\parallel}) m_x(x)\Big|_{x=\pm d/2} \\ \pm A\frac{\partial m_y}{\partial x}\bigg|_{x=\pm d/2} &= K_{\text{S}}^{\parallel} m_y(x)\Big|_{x=\pm d/2}\end{aligned} \tag{13}$$

where $K_{\text{S}}^{\perp}$ is the constant of out-of-plane surface anisotropy and $K_{\text{S}}^{\parallel}$ is the constant of in-plane surface anisotropy. For simplicity in (13) we have assumed that $K_{\text{S}}^{\perp}$ and $K_{\text{S}}^{\parallel}$ are the same for both surfaces. Note that surface anisotropy enters via the boundary condition and not via the equation of motion.

The boundary conditions restrict possible values of k_x, resulting in their quantization. Indeed, substituting (6) in (13) one has [17, 18, 19]

$$(\xi^2 - k_x^2)\tan(k_x d) = 2k_x\xi \tag{14}$$

where the pinning parameter $\xi = (K_{\text{S}}^{\perp} + K_{\text{S}}^{\text{I}})/A$ for the x component of the magnetization and $\xi = K_{\text{S}}^{\text{I}}/A$ for the y component. The solutions of (14) can be numbered by $n = 0, 1, 2, \ldots$ in the increasing order of k_x. Each value of n (and consequently k_x) corresponds to a definite mode of the spectrum of exchange magnetic excitations. The frequency of the excitation, determined by the left-hand side of equation (12), is equal to $\Omega_{\text{ex}} = \Omega_H + \alpha k_x^2 + \alpha k_\parallel^2$. Naturally, the dipole interaction written in the right-hand side of equation (12) disturbs this spectrum. However, for not-too-thick films the dipolar term is small in comparison with the difference between the frequencies of various exchange modes. Thus, one can apply perturbation theory. The zero-order approximation, which includes the diagonal matrix elements of the dipolar interaction, gives renormalization of the frequencies Ω_{ex} and results in the dipole-exchange modes.

To demonstrate this approach consider the case when the surface anisotropy is neglected, i.e. $K_S^{\perp} = K_S^{\parallel} = 0$. Then, from equation (14) one has $k_x = \pi n/d$ ($n = 0, 1, 2, \ldots$). The solutions of (12) are given by

$$\Omega_n^2 = \left[\Omega_{ex} + 1 - p\left(1 - \frac{2p}{1+\delta_{0n}}\frac{1-(-1)^n\exp(-k_\parallel d)}{k_\parallel d}\right)\right] \times \left[\Omega_{ex} + q\left(1 - \frac{2p}{1+\delta_{0n}}\frac{1-(-1)^n\exp(-k_\parallel d)}{k_\parallel d}\right)\right] \tag{15}$$

where $p = k_\parallel^2/(k_\parallel^2 + k_x^2)$ and $q = k_y^2/(k_\parallel^2 + k_x^2)$. The dipole-exchange excitations represent the infinite number of modes ($n = 0, 1, 2, \ldots$). The frequencies of these modes (15) for $n = 0, 1, 2$ as a function of d and $k_\parallel$ are plotted in figure 2. If $n \neq 0$ they are standing bulk spin waves that have cosinusoidal amplitude profiles across the film. In the thin-film limit ($d \to 0$) the frequencies of the bulk modes with $n \neq 0$ become large due to increasing k_x (see figure 2). By contrast, as is seen from (15) the frequency of the lowest mode Ω_0 with $n = 0$ depends only on $k_\parallel$ and is independent of k_x. Therefore, it remains finite at $d \to 0$ (figure 2). As it is explained in [20] the $n = 0$ mode represents a unique bulk spin wave for longitudinal propagation, i.e. for $k_y = 0$ (in this case there is no surface mode). However, it is converted to the surface mode as one swings the propagation vector over the transverse direction for which $k_z = 0$. The frequency of the surface and bulk spin waves depends on the propagation direction through dipolar interactions and is the largest for propagation perpendicular to the applied field. When $k_\parallel = k_y$ and $k_\parallel d$ is small, the frequency of the surface mode Ω_0 coincides with that (9) obtained in the dipolar approximation.

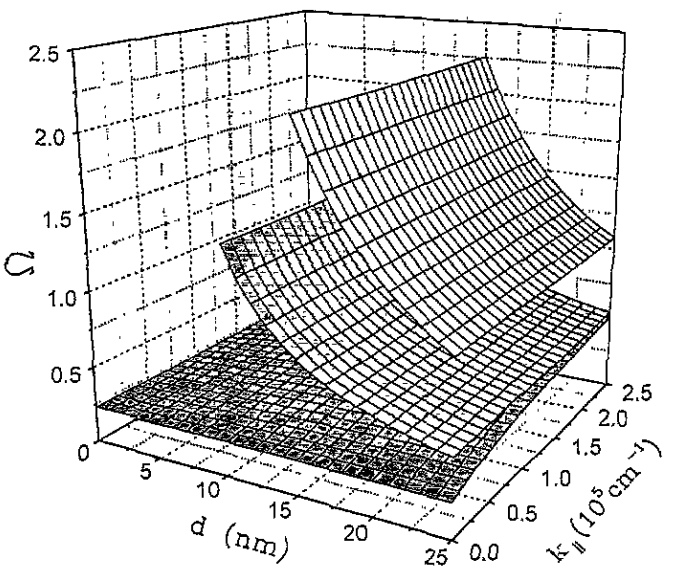

Figure 2. Frequency spectrum of a ferromagnetic slab over the d–$k_\parallel$ plane for the perpendicular propagation of spin waves ($k_\parallel \perp M_0$). The lowest sheet corresponds to the surface mode, while the two upper sheets relate to the low-frequency bulk modes.

Now we will discuss the conditions of applicability of the perturbation theory. It is valid when the frequency difference between various exchange branches is more than matrix

elements of the dipolar interaction. The latter can be evaluated using results of [11] and they are of the order of $k_\parallel d$. Then, for the non–degenerate case, i.e. far from mode crossings, one obtains

$$k_\parallel d < \left(\frac{2A}{4\pi M_0^2}\right)\frac{\pi^2}{d^2}. \tag{16}$$

For typical values of A and M_0 and for the wavevectors $k_\parallel \sim 10^5 \mathrm{cm}^{-1}$, relation (16) is satisfied if the film thickness d is of the order or less than 20 nm.

If d is small, i.e. $\xi d \ll 1$, one can easily find the influence of the surface anisotropy on the spectrum of magnetic excitations. In this case, as follows from (14), $k_x^2 = -2\xi/d$ for the mode with $n = 0$. Then, using (15) and neglecting the terms, proportional to ξd, one has for the surface mode

$$\Omega_0^2 = \left[\Omega_H + \alpha k_\parallel^2 - \frac{K_S^\perp + K_S^\parallel}{\pi M_0^2 d} + \frac{1-\exp(-k_\parallel d)}{k_\parallel d}\right] \times \left[\Omega_H + \alpha k_\parallel^2 - \frac{K_S^\parallel}{\pi M_0^2 d} + \frac{k_y^2}{k_\parallel^2}\left(1 - \frac{1-\exp(-k_\parallel d)}{k_\parallel d}\right)\right]. \tag{17}$$

This result is in agreement with that obtained by Stamps and Hillebrands [21] in the limit of $k_\parallel d \ll 1$ and $K_S^\parallel = 0$.

Note that the surface anisotropy appears in (17) as an effective bulk anisotropy. This feature is often used for the practical evaluation of surface anisotropies from experimental data. However, it should be mentioned that such an approach is correct only if the film thickness d is less than the magnetic length $\sqrt{\alpha}$.

Now we consider *ferromagnetic bilayer system* as represented in figure 3, where there are two magnetic layers of thicknesses d_1 and d_2 separated by a non-magnetic spacer of thickness d_0. If d_0 is much more than a typical wavelength of spin waves then two magnetic layers can be considered independently. In experiments on light scattering this distance is determined by the value $k_\parallel^{-1}$ and is of the order of 100 nm. Then the spectrum of magnetic excitations can be described by means of the theory given above. At smaller distances d_0 the dipole coupling between the magnetic layers is essential and should be taken into account. Detailed study of this case in an approximation where exchange and anisotropies are neglected has been carried out in papers [22, 23, 24].

The main results of these studies can be summarized as follows. If $k_\parallel$ is perpendicular to the magnetizations lying in plane of the two layers the frequencies of the magnetostatic modes are [22]

$$\Omega = \sqrt{(\Omega_H + \tfrac{1}{2})^2 - \tfrac{1}{4}\beta} \tag{18}$$

The quantity β is equal to unity for a bulk mode, giving the same result as that for a single film (equation (7) with $k_z = 0$). For the surface modes β takes on two values depending on $k_\parallel$, d_0, d_1 and d_2. In the limit of large separation of the magnetic layers ($d_0 \to \infty$) β becomes equal to $\exp(-2k_\parallel d_1)$ and $\exp(-2k_\parallel d_2)$. The relating frequencies obtained from (18) are just the surface magnetostatic mode frequencies for single films of thickness d_1 and d_2, as can be seen by comparison with (9). In the opposite limit of $d_0 \to 0$ one can obtain $\beta = 1$ and $\beta = \exp[-2k_\parallel(d_1 + d_2)]$. The first solution represents a mode that has become degenerate with the bulk magnons, while the second solution corresponds to the

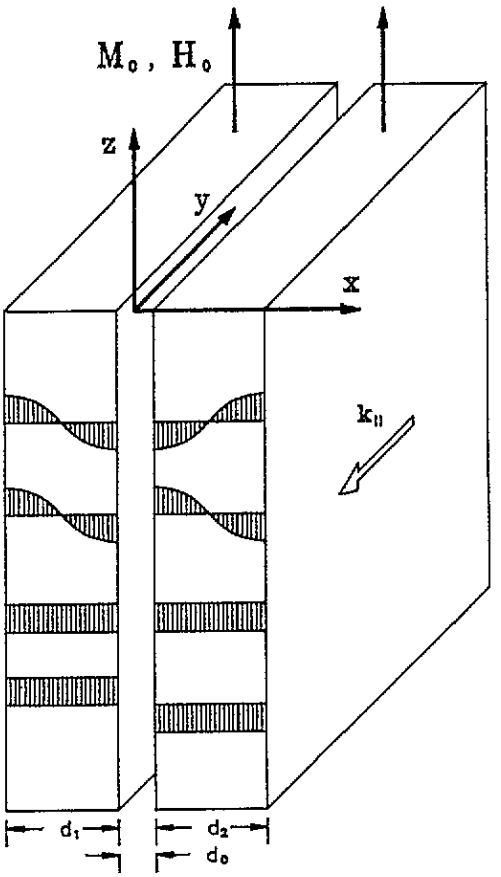

Figure 3. Bilayer consisting of two ferromagnetic layers with thicknesses d_1 and d_2 separated by a non-magnetic spacer layer of thickness d_0. Profiles of various types of spin wave in the case of zero interlayer exchange coupling $A_{12} = 0$ are schematically shown.

surface mode for the layer of overall thickness $d_1 + d_2$. The behaviour of the magnetistatic mode frequencies for $d_1 = d_2 = d$ is demonstrated in figure 4.

When the thickness of the non-magnetic spacer becomes 5 nm or less a short-range interlayer exchange coupling appears and transforms the spectrum of magnetic excitations. In this case frequencies of spin waves depend on the type of interlayer exchange and are different for ferromagnetic, antiferromagnetic and 90° exchange coupling. Interlayer ferromagnetic exchange was treated theoretically in [12, 25–28] and is considered below. In the range of distances between magnetic films $d_0 < 5$ nm the dipolar interlayer interaction remains practically in saturation and does not depend on d_0. Therefore, we can let $d_0 = 0$.

In contrast to intralayer exchange which enters both into the Landau–Lifshitz equation and into the Rado–Weertman boundary condition, interlayer exchange, due to its local character, appears only in boundary conditions at the interface. The latter were introduced for the first time by Hoffmann [29]. For the long-wavelength limit considered here, the linearized version of the Hoffmann boundary conditions is

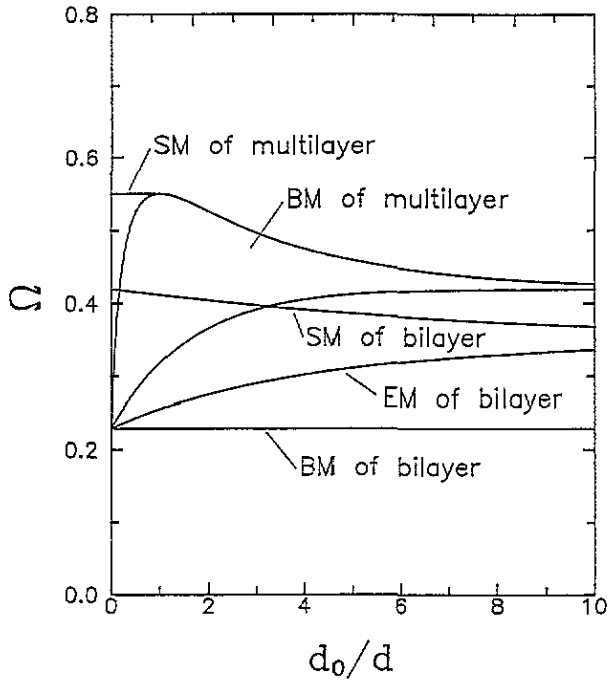

Figure 4. *Magnetostatic mode frequencies of bilayer and multilayer for $\Omega_H = 0.05$, $d = 10$ nm and $k_\parallel = 1.7 \times 10^5$ cm^{-1} versus d_0/d.* SM and BM denote the surface and the bulk modes respectively. EM indicates the exchange-sensitive mode of the bilayer.

$$A\frac{\partial m_{1x}}{\partial x} + A_{12}[m_{1x}(x) - m_{2x}(x)]\Big|_{x=0} = 0$$
$$A\frac{\partial m_{2x}}{\partial x} + A_{12}[m_{1x}(x) - m_{2x}(x)]\Big|_{x=0} = 0. \tag{19}$$

Here m_{1x} and m_{2x} are fluctuating x components of the magnetization of the first and the second film respectively. In equations (19) we have assumed for simplicity that the saturation magnetizations and exchange stiffnesses of the two magnetic films are the same and the anisotropy at the interface is neglected. Analogous relations can be written for y components of magnetization. At the external surfaces the Rado–Weertman boundary conditions have to be fulfilled. If the surface anisotropy is equal to zero they are

$$\frac{\partial m_{1x}}{\partial x}\Big|_{x=\pm d} = 0 \qquad \frac{\partial m_{2x}}{\partial x}\Big|_{x=\pm d} = 0 \tag{20}$$

where we let $d_1 = d_2 = d$, assuming the same thicknesses of the magnetic films. Analogous relations can be written for m_{1y} and m_{2y}. Representing $m_{1x}(x)$ and $m_{2x}(x)$ in analogy with (6) as a sum of two oscillating functions one can easily derive from (19) and (20) the condition of quantization for k_x:

$$k_x - k_x \cos(2k_x d) - \frac{2A_{12}}{A}\sin(2k_x d) = 0. \tag{21}$$

There exist two kinds of solutions of equation (21). The first one is $k_x = (\pi n)/(2d)$ ($n = 0, 2, 4, \ldots$). It corresponds to the so-called in-phase solution at which the mode profiles are continuous at $x = 0$. This solution does not depend on the strength of the interlayer coupling A_{12} and coincide with that obtained for the single magnetic film with the thickness equal to $2d$ and even n (see figure 5). If $n \neq 0$ it relates to standing bulk spin waves, that have continuous cosinusoidal amplitude profiles across both films. If $n = 0$ and $k_\parallel = k_y$, the solution represents the surface mode. Neglecting the term $\alpha k_\parallel^2$, its frequency at small $k_\parallel d$ can be written as follows:

$$\Omega_0^2 = \left[\Omega_H + 1 - k_\parallel d\right]\left[\Omega_H + k_\parallel d\right]. \tag{22}$$

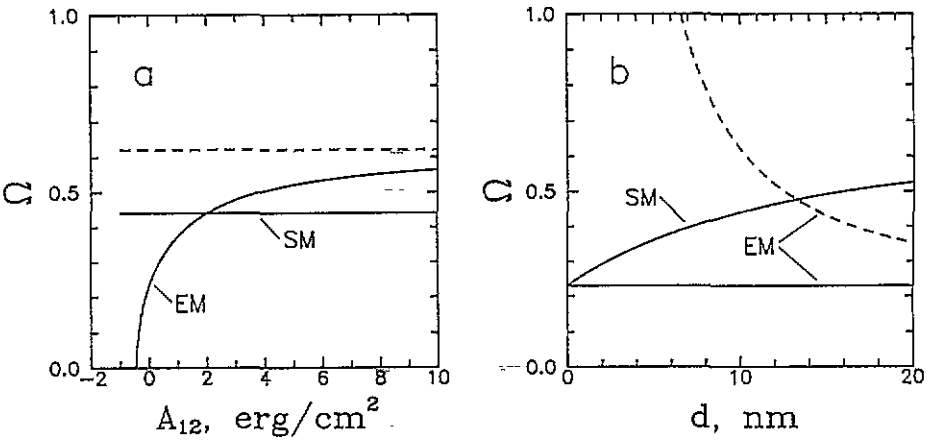

Figure 5. Frequencies Ω of the exchange-sensitive mode (EM) and the surface mode (SM) of a ferromagnetic bilayer with the equal thicknesses $d_1 = d_2 = d$ for $\Omega_H = 0.05$. (a) Ω against A_{12} for $d = 10$ nm. The dashed line marks the frequency of the lowest bulk mode of a single film of thickness $2d$ and corresponds to the exchange mode of the bilayer in the limit $A_{12} \to \infty$. (b) Ω against d for $A_{12} = 0$. EM transforms with increasing A_{12} and in the limit $A_{12} \to \infty$ it is given by the dashed line.

Another kind of solution represents the so-called out-of-phase mode and strongly depends on the value of the interlayer coupling A_{12}:

$$\Omega_1^2 = \left[\Omega_H + \alpha k_x^2 + 1\right]\left[\Omega_H + \alpha k_x^2\right] \tag{23}$$

where k_x is the root of equation (21) corresponding to this solution. It changes from $k_x = (\pi n)/(2d)$ ($n = 0, 2, 4, \ldots$) at $A_{12} = 0$ to $k_x = (\pi n)/(2d)$ ($n = 1, 3, 5, \ldots$) at $A_{12} \to +\infty$.

If $A_{12} = 0$ the phases of $m_1(x)$ and $m_2(x)$ are opposite. For the lowest mode $k_x = 0$. However, as it is seen from equations (22), (23) the frequencies of in-phase and out-of-phase modes are different. The reason of that is the difference in the energy of the dipolar coupling between two films. This energy is more for in-phase fluctuations of the magnetizations than for out-of-phase fluctuations. For very thin films or/and for long-wave fluctuations this difference is small. The profiles of the in-phase and out-of-phase modes are shown in figure 3.

The increase of the interlayer coupling causes the spins of the two ferromagnetic films at the interface to precess in unison. In this case the mode profile of the out-of-phase solution changes continuously and finally it becomes the mode profile of the exchange mode of the single layer with doubled thickness. It happens when $A_{12} \sim A/a$, where a is the lattice parameter [27]. In this case for the lowest mode one obtains $k_x = \pi/(2d)$.

Frequencies of the two lowest modes versus A_{12} and d are shown in figure 5. They were calculated using (23) and the exact solution of equation (21) and reflect the features of spin waves in bilayers described above. Note that in the region of the mode crossing the resulting solution should be consider as a linear combination of the solutions corresponding to the modes with two different k_x. It would give mode repulsion which was discussed in [27].

Additional peculiarities of the spin-wave spectrum appear in *multilayers*, i.e. a stack consisting of many ferromagnetic layers separated by non-magnetic spacer layers. Dispersion relations for spin waves in such systems (without inclusion of exchange interactions and anisotropies) was studied theoretically in papers [30–33]. Inclusion of volume anisotropy contributions was made in [34]. Below we shall briefly outline the main results obtained in these papers for an infinite number of layers.

For propagation normal to the magnetization in the plane of the layers the spin-wave frequency can be written as (18). The factor β has a complicated form. It depends on the parameters $k_\parallel$, d, d_0, where d and d_0 are the thicknesses of the ferromagnetic and non-magnetic layers, respectively. As it can be shown [30] the spin-wave mode of the stack is a linear superposition of surface waves within each magnetic layer. The bulk modes form a continuous zone and always lie in the frequency range from $[\Omega_H(\Omega_H + 1)]^{1/2}$ to $(\Omega_H + \frac{1}{2})$ (see figure 4). For a finite number of layers N the spectrum of bulk modes represents N branches lying inside the bulk zone shown in figure 4. The surface mode of the superlattice is also a linear superposition of surface waves within each magnetic layer. However, it exists only if the magnetic layer thickness is greater than the spacer layer thickness $d > d_0$. The frequency of the surface mode is equal to $(\Omega_H + \frac{1}{2})$, i.e. it is the same as that in a semi-infinite ferromagnet. As $d \to d_0$, the attenuation constant of the surface mode tends to zero, and the frequency of the surface wave merges with the top of the band of bulk collective modes (see figure 4). The surface mode is predicted to have 'one-way' propagation only as for the thin film.

Exchange modes in multilayered systems, in the approximation that interlayer exchange and anisotropies are neglected, were considered in [12, 25, 35, 36]. For a multilayer consisting of N ferromagnetic films magnetized in plane, each branch of the corresponding single-film spectrum splits into N branches due to formation of the collective modes of the stack. The frequencies of the spin waves depend on the direction of the wavevector relative to the magnetization M_0. For a given $|k_\parallel|$, when the direction of propagation changes from longitudinal to transverse, the frequency of the spin wave, corresponding to the particular branch of the spectrum, gradually increases [12]. At $d \to 0$ all modes become degenerate. However, the surface-mode frequencies remains finite while the frequencies of the bulk exchange modes become infinite as occurs in bilayers.

A detailed theoretical description of the behaviour of the dipole-exchange modes in the presence of anisotropies and interlayer coupling was given in the work of Hillebrands [37, 28]. Using numerical calculations, based on the straightforward solution of the equation of motion for the magnetization and exact boundary conditions, he was able to calculate the spin-wave frequencies in multilayered systems practically for all possible real situations. Recently, the influence of imperfections of an ultra-thin ferromagnetic film on spin-wave propagation was reported [38].

3. Light scattering from spin waves

The microscopical origin of light scattering from spin waves is the spin–orbital and exchange interactions. First detailed calculations for the spin–orbital mechanism on the basis of microscopic theory were performed by Shen and Blombergen [39] and Fleury and Loudon [40]. They derived the relation between the light scattering intensity and the matrix elements of the spin–orbital interaction between different excited states of an individual ion. To overcome the difficulties associated with the calculation of the matrix elements, the phenomenological expansion of the crystal permittivity ϵ in the spin operators (or the magnetization) was proposed [41, 42]. The consistent presentation of this calculation can be found in [43]. Light-scattering theory involving surface effects has been given in [44–46]. Recent calculations take into account surface and bulk anisotropies and enable the quantitative comparison of the theory with experimental results obtained for real systems [47, 48].

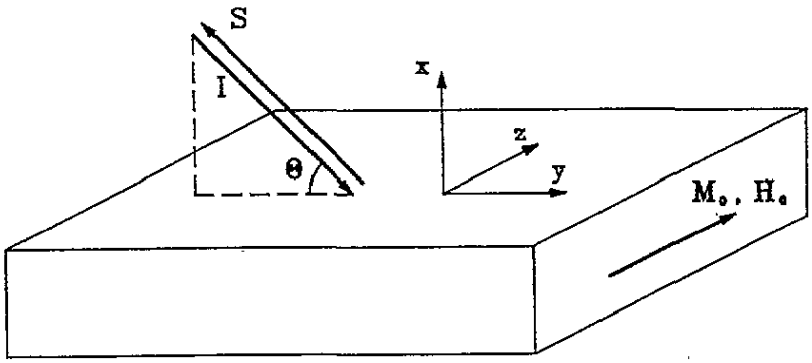

Figure 6. Typical geometry of the BLS experiment on thin films. The incident (I) and scattered (S) light beams for the 'backscattering' are indicated. Changing θ allows the variation of $k_{\|}$.

Let us consider an experimental situation as represented schematically in figure 6. Monochromatic light of angular frequency $\omega_I = 2\pi\nu_I$ is incident on the scattering medium, which could be characterized by its dielectric permittivity tensor $\epsilon^{\alpha\beta}$. The electric field vector $\boldsymbol{E}_I$ is polarized in the direction of the unit vector $\boldsymbol{e}_I$, and the direction of the incident light beam is parallel to the wavevector $\boldsymbol{k}_I$ in the medium. The incident electric field $\boldsymbol{E}_I$ induces a polarization $\boldsymbol{P}$ in the medium. The effect of magnetic excitations is to modulate the dielectric permittivity and hence to produce a fluctuating term in the polarization, $\delta\boldsymbol{P}$

$$\delta P^{\alpha}(r,t) = \sum_{\beta} \frac{\delta\epsilon^{\alpha\beta}(r,t)}{4\pi} E_I^{\beta}(r,t) \tag{24}$$

where $\delta\epsilon^{\alpha\beta}$ is the fluctuating part of $\epsilon^{\alpha\beta}$. This in its turn gives rise to a scattered electromagnetic wave whose electric field $\boldsymbol{E}_S$ and frequency $\omega_S = 2\pi\nu_S$ can be calculated from Maxwell's equations. The scattering process is inelastic in general ($\omega_I \neq \omega_S$) because an incident photon of energy $\hbar\omega_I$ may take energy from, or give energy to, an excitation in the medium in order to produce the scattered photon of energy $\hbar\omega_S$.

The light may be scattered in many different directions and with different frequencies. The experiment, however, is normally designed such that only the scattered light of

wavevector k_S frequency ω_S, and electric field polarization e_S arrives at the detector. The spectrum of the scattered light is obtained by measuring the *differential extinction coefficient* $dh/d\Omega\, d\omega_S$. This quantity is defined as follows: dh is the ratio of the number of photons scattered into an elementary solid angle $d\Omega$ with a scattered frequency between ω_S and $\omega_S + d\omega_S$, per unit time and volume, to the incident photon flux density [49]. Instead of differential extinction coefficient the *differential scattering cross section* [5], which is directly connected to the former, is often used.

Derivations of $dh/d\Omega d\omega_S$ for light scattering in an unlimited medium have been given in a number of textbooks (see, for example, [49] for a detailed account). In the case of scattering with small change of frequency it can be represented as follows:

$$\frac{dh}{d\Omega\, d\omega_S} = \frac{\omega_I^4}{32\pi^2 c^4} \sum_{\alpha\beta\alpha'\beta'} e_I^\alpha e_S^\beta e_I^{\alpha'} e_S^{\beta'} \langle (\delta\epsilon_k^{\alpha\beta})^* \delta\epsilon_k^{\alpha'\beta'} \rangle_\omega \tag{25}$$

where the wavevector k and frequency ω are given by

$$k_S = k_I - k \qquad \omega_S = \omega_I - \omega \tag{26}$$

and the correlation function is defined by the transformation

$$\langle (\delta\epsilon_k^{\alpha\beta})^* \delta\epsilon_k^{\alpha'\beta'} \rangle_\omega = \int\int dt\, d^3(r_2 - r_1) \exp[i\omega t - ik \cdot (r_2 - r_1)] \langle [(\delta\epsilon^{\alpha\beta}(r_1, t)]^* \delta\epsilon^{\alpha'\beta'}(r_2, 0) \rangle \tag{27}$$

where $\langle ... \rangle$ denotes statistical (and, if necessary, quantum-mechanical) averaging.

If k and ω are interpreted as the total wavevector and frequency of the crystal excitation that participate in the scattering process, then equations (26) are simply the conditions for conservation of the momentum and energy, respectively. For $\omega > 0$ ($\omega_S < \omega_I$) this is a Stokes scattering process in which the energy is removed from the incident beam in order to create an excitation in the scattering medium. On the other hand $\omega < 0$ ($\omega_S > \omega_I$) corresponds to an anti-Stokes process in which the scattered photons are more energetic than the incident photons because of the energy gained from the crystal excitation. Thus, changing the experimental geometry, one can investigate by means of light scattering spin waves with different k. For example, when the angle φ between k_I and k_S is small (the so-called 'forward scattering') spin waves with small $k \sim 10^3$–$10^4 cm^{-1}$ are under investigation. On the other hand, the 'backscattering' geometry, shown in figure 6, corresponds to $\varphi = 180°$. In this process the maximum value of k can be reached.

The existence of absorptive media or media with restricted geometry such as a thin film or layered system essentially changes the expression (25) [5]. The main difference arises from the fact that translation invariance holds only in the y–z plane. In this case, the correlation function determining the scattering is

$$\langle (\delta\epsilon_{k_1}^{\alpha\beta})^* \delta\epsilon_{k_2}^{\alpha'\beta'} \rangle_\omega = \int\int dt\, d^2(r_{1\parallel} - r_{2\parallel})\, dx_1 dx_2 \exp[i\omega t - ik_\parallel \cdot (r_{1\parallel} - r_{2\parallel})]$$
$$\times \exp[-i(k_{1x}x_1 - k_{2x}x_2)] \langle [\delta\epsilon^{\alpha\beta}(r_1, t)]^* \delta\epsilon^{\alpha'\beta'}(r_2, 0) \rangle \tag{28}$$

where the 2D wavevector $k_\parallel$ is parallel to the surface, $k_1 = \{k_{1x}, k_\parallel\}$, $k_2 = \{k_{2x}, k_\parallel\}$ and similarly for r_1 and r_2. The wavevector $k_\parallel$ and the frequency ω are determined by the conditions for conservation similarly to (26):

$$k_{S\parallel} = k_{I\parallel} - k_\parallel \qquad \omega_S = \omega_I - \omega. \tag{29}$$

Since the system does not possess a translation invariance symmetry in the x direction, it might be that $k_1 \neq k_2$.

The magnetic contribution to the tensor $\epsilon^{\alpha\beta}$ can be represented as a series in the powers of the magnetization vector M:

$$\Delta\epsilon^{\alpha\beta} = \sum_{\gamma} f^{\alpha\beta\gamma} M_\gamma + \sum_{\gamma\delta} g^{\alpha\beta\gamma\delta} M_\gamma M_\delta. \tag{30}$$

The tensors **f** and **g** are, in general, complex and describe magneto-optical effects. The tensor **f** characterizes circular birefringence (Faraday effect) and linear dichroism, the tensor **g** characterizes linear birefringence and circular dichroism. In the presence of magnetic fluctuations produced by spin waves the value $\Delta\epsilon^{\alpha\beta}$ contains a fluctuating part $\delta\epsilon^{\alpha\beta}$ which determines the correlation function (28). Therefore, the problem of the evaluation of the light scattering intensity is reduced to the calculation of the several correlation functions of the different components of the magnetization. These correlation functions may be calculated with the help of the fluctuation-dissipation theorem [40,48] or by means of a more transparent thermodynamical approach [47].

The calculation of the extinction coefficient for any realistic structure is rather an intricate task and it must be worked out using a computer. For a detailed account we refer the reader to the original works mentioned. The measurement of the absolute value of the light scattering intensity is also very complicated problem. Therefore, the relative BLS intensity and its variation as a function of some parameters (e.g. applied field, light polarization, temperature etc) is commonly investigated. Below we consider a few particular features of light scattering from spin waves, which are points of interest.

Usually, the tensors **f** and **g** have off-diagonal non–zero coefficients. This means that the correlation function with off-diagonal $\delta\epsilon^{\alpha\beta}$ contributes to light scattering from spin waves and the scattering takes place with rotation of the polarization plane. This feature is used to distinguish between BLS from phonons and spin waves and to increase the effective contrast of a spectrometer (see subsection 4.2). However, this is not always the case. There exists a specific exchange light-scattering mechanism, which results in the contribution of the spin-wave fluctuations only to the diagonal components of the tensor $\epsilon^{\alpha\beta}$ [51]. This causes the scattering without rotation of the polarization plane. This mechanism is of decisive importance for strongly canted magnetic systems, such as antiferromagnets in a high applied magnetic field. But it can also appear in multilayer structures with AF-type exchange.

Now we consider the relation between the extinction coefficients for Stokes and anti-Stokes processes. *Four causes for the asymmetry of Stokes–anti-Stokes line intensity* are known. The first one is connected with the thermal population of the magnon states. It can be deduced from the principle of detailed balancing [49] and involves the consideration of time-reversal properties. It can be shown that it is more probable to create a spin wave (Stokes process) than to destroy one (anti-Stokes process). The corresponding Stokes–anti-Stokes ratio can be expressed as follows:

$$\frac{dh_{\text{Stokes}}}{dh_{\text{a-Stokes}}} = \exp\left(\frac{\hbar\omega}{k_B T}\right) \tag{31}$$

where ω is the spin-wave frequency, k_B is Boltzmann's constant and T is the temperature. This mechanism would be the only reason to cause the Stokes–anti-Stokes difference if the ground state did not change under time reversal. In magnetic systems this is not the case,

and this leads to a more complicated relation than formula (31). However, under some circumstances (see [5]) the relation (31) is valid.

The second cause for the asymmetry can be explained as follows. Let us consider a magnetic solid which possesses both the linear $\mathbf{f}$ and the quadratic $\mathbf{g}$ magneto-optical constants (see (30)). It is possible to show [43] that, if $e_I \| M$ and $e_S \perp M$, than on the Stokes side of the spectrum the linear and biquadratic terms interfere constructively, and $dh \sim |\mathbf{f} + iM\mathbf{g}|^2$. On the anti-Stokes side the two terms interfere destructively, and $dh \sim |\mathbf{f} - iM\mathbf{g}|^2$. If both e_I and e_S are rotated through 90°, the constructive and destructive interference will take place for anti-Stokes and Stokes processes respectively.

These two mechanisms, the thermal population and the interference of the linear and the quadratic contribution, have one common feature. A reversal of the magnetization does not change the Stokes–anti-Stokes ratio.

The third cause is revealed in the BLS from surface spin waves. The feature of the surface excitation is its localization near one of the surfaces. As was illustrated in figure 1 the surface spin wave propagating along the y direction has its largest amplitude near the right-hand surface. The surface spin wave, propagating in the opposite direction, is localized on the lefthand surface. Due to this inreciprocity and the finite penetration depth of the incident light the scattering with creation of the surface excitation differs from that with destruction of the surface excitation. Since a reversal of the magnetization causes a reversal of the localization of the surface spin waves there will also be a reversal in the Stokes–anti-Stokes ratio. Such a mechanism was experimentally observed in [52]. Nowadays, this feature of the BLS is often used for the identification of peaks corresponding to surface spin waves in complex BLS spectra.

In the case of very thin films, when the thickness of the film is much smaller then the localization length of the surface spin waves, the localization mechanism does not cause the Stokes–anti-Stokes asymmetry. However, if the light absorption is high enough, the contribution of the off-diagonal spin–spin correlation functions to the light scattering intensity becomes important. It results in the different intensity of the Stokes and the anti-Stokes lines [46]. A reversal of the magnetization reverses the Stokes–anti-Stokes ratio, although the change of the spin-wave localization in such thin films is negligible.

To conclude this section we note that there are several experimental observations relating to the Stokes–anti-Stokes asymmetry, which are waiting for a theoretical explanation. The change in the Stokes–anti-Stokes ratio in BLS on the Fe/Cr/Fe layered system with variation of Cr interlayer thickness is among them. Another example will be given in section 7.

4. Experimental methods

For the successful exploration of the magnetic excitations in layered structures by means of BLS high-quality thin films as well as a spectrometer with high resolution and sensitivity are necessary. In this section experimental methods for thin-film preparation and Brillouin spectroscopy are considered.

4.1. Preparation and characterizing of thin films and layered systems

Preparation and characterization of thin magnetic films is now a vast field which cannot be exhaustively reviewed in the present paper. A detailed analysis of this subject is presented, for example, in [53, 54]. We only describe general concepts and introduce terms which will be used below.

Molecular beam epitaxy (MBE) is a very popular technique for the preparation of thin magnetic films. Its advantage is the possibility of producing well defined high-quality monocrystalline films and layered systems with a small number of defects and impurities. Ultra-high-vacuum (UHV) chambers with basic pressure better than 10^{-10} mbar are commonly used for film preparation. A standard part of such UHV systems is a special transfer chamber. This allows one to introduce substrates into the main chamber and to take grown films out without breaking the UHV. After the introduction into UHV the substrate should be cleaned to remove surface layers, which are oxidated or damaged by fabrication. This is usually done by annealing in UHV or by argon ion sputtering.

For the realization of MBE the choice of substrate material and deposition temperature is of special importance. To produce well defined thin films or layered systems one needs to establish an epitaxial layer-by-layer-mode growth, i.e. a growth when the successive layer begins to grow after the completion of the previous one. For that free surface energies of the substrate and the deposited material as well as their interface energy and the growth rate should satisfy specific thermodynamic and kinetic relations [55]. Another essential parameter determining epitaxial growth is the lattice misfit f. It is defined as $f = (b - a)/a$, where b and a are the lattice parameters of the film and the substrate, respectively. Good epitaxial growth is expected when the overlayer and substrate lattice meshes are well matched, i.e. the misfit is small (of the order of 1% or smaller, e.g. in the case of Al or Cr on Fe(001)). However, epitaxial growth with higher misfit was reported in [53].

Interdiffusion also plays an important role in the process of the thin-film deposition. In an ideal situation interdiffusion of the substrate and the film should be forbidden by the phase diagram. This is the case, for example, for Fe on Ag and Cu. Nevertheless, one can avoid essential interdiffusion even for a system where it is not forbidden (e.g. Fe on Au) by decreasing the substrate temperature during the growth process. Therefore, choosing the best growth temperature is extremely critical. One wants a high enough temperature to allow movement of atoms to provide crystal quality yet low enough to prevent interdiffusion.

It is virtually impossible to select appropriate MBE conditions without *in situ* monitoring of the growth. Therefore, the MBE chambers are usually equipped with some of the surface investigation tools, such as low energy electron diffraction (LEED), reflection high energy electron diffraction (RHEED), Auger electron spectroscopy (AES) and scanning tunneling microscopy (STM).

In LEED studies the sample is irradiated, mostly at normal incidence, by a low-energy electron beam (of the order of 100 eV). The elastically scattered electrons are visualized and used for the structural analysis. The following information can be obtained from a LEED experiment: firstly, the spot pattern indicates crystalline order and its symmetry and its variation with changing electron energy reflects the symmetry of the sample; secondly, the small-angle analysis of a given spot makes it possible to determine the real structure of the surface under investigation, i.e. the shape of growing islands, the distance between terraces, etc.

The RHEED diffraction pattern can be visualized if electrons with energy of 10–20 keV are reflected from the crystalline surface after glancing incidence. In principle, this technique provides the same information about the symmetry of the surface as LEED. However, RHEED patterns are more sensitive to surface roughness, although the quantitative analysis is more complicated than in case the of LEED. The alternative changing of both RHEED and LEED patterns during the deposition can be used for layer-by-layer growth monitoring and precise measuring of thin-film thicknesses.

STM (or its modification—atomic force microscopy, which makes it possible to study

isolators) provides detailed information on epitaxial growth and the morphology of film surfaces. This technique is unique in terms of its atomic resolution and its visualizability. The application of STM to the investigation of the magnetic properties of surfaces is in progress.

The AES technique differs from the others by its sensitivity to the chemical composition of the surface, because the energy of Auger electrons depends only on the kind of atom they are emitted from. Moreover, their penetration depth is less than 1 nm. Therefore, the measurement of the intensity of the Auger electrons, emitted by atoms of substrate during the growth can be used for the determination of the type of growth. Observation of the so-called 'Auger kinks' is an evidence of layer-by-layer growth.

The detailed description of the above-cited techniques is far beyond the scope of the paper. We refer the reader to [53] and references therein.

Among achievements of the MBE technique in preparation of thin magnetic films and layered systems with almost perfect crystallinity we can mention BCC Co on GaAs(110) [56], FCC Co on Cu(001) [57], Fe on W(110) [58], Fe on Ag [59] and FCC Fe on Cu [60], Fe/X/Fe (X=Cr,Al,Ag,Au) on silver buffer with GaAs as a substrate [61], Fe/X/Fe (X=Cr,Ag,Au) directly on an Fe whisker [62–64] and many others (see [53]).

Cathode sputtering is also applied to preparation of layered systems. It has the advantage of applicability to various materials. This method could be automated, which is a matter of importance in preparation of multilayered systems with as many as 100 individual magnetic and non–magnetic layers. The advantage of sputtering is clearly demonstrated in [65] where the preparation and investigation of a series of layered structures Fe/X/Fe, X being almost all d metals, are reported. The disadvantages of cathode sputtering are the unavoidable contamination of the growing films by a gas, in which discharge is sustained, and the impossibility (with a rare exception) of producing monocrystalline samples.

It is necessary to emphasize that light-scattering experiments are mainly performed on monocrystalline MBE-grown samples. In this case one can avoid the huge broadening of a spectrum due to distribution of the anisotropy axis directions which takes place in polycrystalline samples. Moreover, performing experiments on monocrystalline samples one has the possibility of applying the magnetic field along different directions relative to the crystallographic axis. This increases the body of information obtained in the experiments and makes its theoretical interpretation more straightforward. There are, nevertheless, a few BLS experiments on polycrystalline films which will be described in the respective section.

Besides good crystallinity optical properties are an important characteristic of the layered systems used in light-scattering experiments. The reduction of reflection on the film surface brings about increasing light scattering intensity and therefore is very desirable. For this purpose anti-reflection layers can be deposited on the film after its preparation. For example, a ZnS overlayer with a thickness of about 50 nm increases the BLS intensity in Fe films and Fe-based layered systems five to seven times.

4.2. Techniques for investigation of light scattering

A general view of the installation required to carry out Brillouin light scattering (BLS) experiments is shown in figure 7. It consists of four main parts: the laser source, the spectrometer, the detector and the electronic system for data acquisition and control.

The main requirement to the laser source is that its generation should be well polarized and the corresponding spectral linewidth is to be much smaller than 1 GHz. This restriction results from the typical frequency shift in BLS (5–50 GHz), which is determined by the frequency of the quasi-particle, taking part in the BLS process. Such a condition is satisfied only by the gas lasers. Usually, standard He–Ne lasers have a linewidth of about 200 MHz.

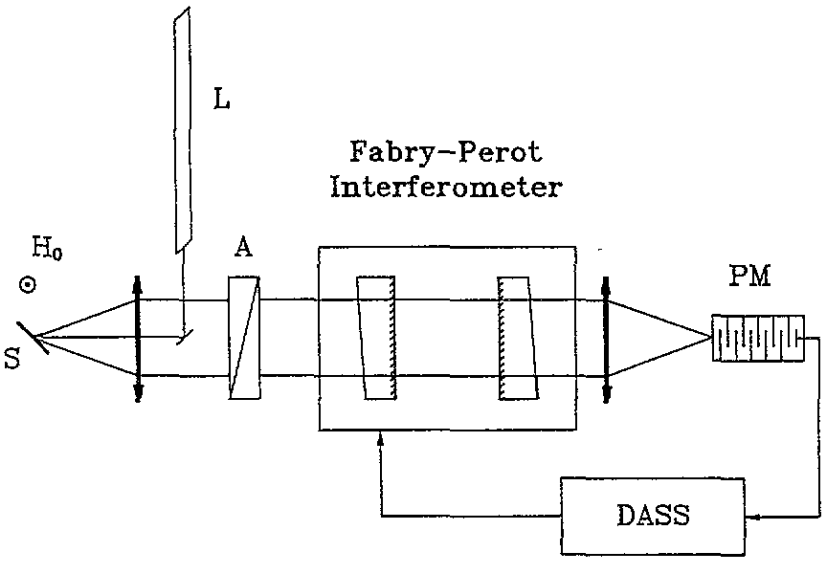

Figure 7. Schematic representation of the equipment used for Brillouin light scattering. L is the laser source, S the sample, A the polarization analyser, PM the photomultiplier, DASS the data acquisition and stabilization system. H_0 denotes the applied magnetic field.

They can be used without any modification, if the extremely high-frequency resolution is not necessary. Ar^+ and Kr^+ lasers have a linewidth of more than 5 GHz. They cannot be applied directly, their generation frequency must be stabilized to a single mode of the laser cavity. This is usually done by introducing a quartz Fabry–Pérot etalon into the laser cavity. In this case the linewidth of Ar^+ and Kr^+ lasers becomes of about 20 MHz. Such lasers can be used for high-resolution experiments.

Because of the small frequency shift in the Brillouin light-scattering process a spectrometer with extremely high resolution, namely scanning Fabry–Pérot interferometer (FPI), is applied to analysing the scattered light. For a better understanding of the processes involved let us consider the operation of the FPI in more detail. It is based on two parallel flat mirrors, d being the separation between the reflecting surfaces of the mirrors. With parallel light incident on the mirrors at angle ϕ the maximum transmitted frequency ν_m is given by interference conditions

$$m\frac{c}{\nu_m} = 2nd\cos\phi \tag{32}$$

where $m = 0, 1, 2, \ldots$ is the order of the interference, n is the refractive index of the medium between the mirrors (usually $n = 1$ for air) and c is the speed of light. The frequency dependence of the FPI transition at a given distance between mirrors is presented in figure 8. We draw attention to the three points of importance that are seen in figure 8. Firstly, the transmission condition is satisfied for a whole series of frequencies ν_m which correspond to the different orders of the interference. The frequency difference $\Delta\nu = \nu_m - \nu_{m+1}$ is called the free spectral range (FSR) and it is

$$\Delta\nu = \frac{2c}{nd}. \tag{33}$$

For the typical distance of $d = 3$ mm the FSR is equal to 50 GHz. Secondly, the transmission peaks have a linewidth ($\delta\nu$), which depends on many parameters, but for a typical experimental situation $\delta\nu \simeq 1$ GHz. Thirdly, even if condition (32) is not satisfied, the transmission of FPI $T(\nu)$ is not zero ($T_{\min}$ in figure 8). The ratio of the maximum transition to the minimum one $T_{\max}/T_{\min}$ is called the contrast of interferometer. Usually, this value is limited to 10^2–10^3. This means that lines with intensity smaller than 10^{-3}–10^{-2} of the unavoided background, caused by elastic scattering, cannot be detected by the FPI, since the background is suppressed only by a factor of the contrast.

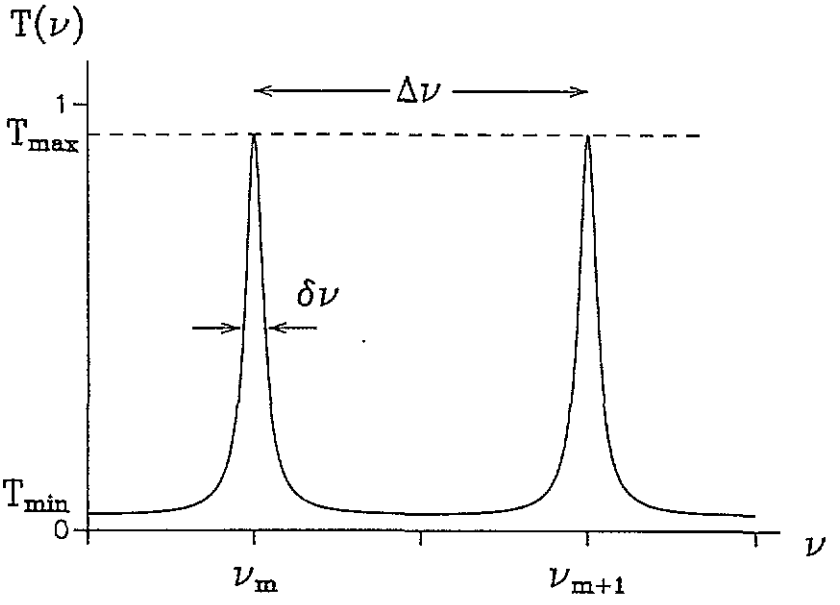

Figure 8. Transmission of the Fabry–Pérot interferometer as a function of the incident light frequency. Frequencies ν_m and ν_{m+1} correspond to different orders of the interference. The resolution of the interferometer is determined by the linewidth $\delta\nu$, the free spectral range (FSR) is equal to $\Delta\nu$, and the ratio $T_{\max}/T_{\min}$ gives the contrast.

It is clear from above that FPI permits the resolution of spectral lines with frequency shifts corresponding to BLS from spin waves. However, the small intensity of Brillouin lines (10^{-10}–10^{-8} of the incident beam) and considerable Rayleigh (elastic) scattering (10^{-4}–10^{-2} of the incident beam) in magnetic solids are specific features of this process. This means that the contrast of the interferometer is too low to allow BLS to be seen. The intensity of the Rayleigh line could be considerably reduced by introducing a polarization analyser between the sample and the interferometer (see figure 7). This does not reduce light scattered from spin waves, since such scattering rotates a polarization plane (see section 3). However, even after that, it is too high to be sufficiently suppressed by a standard FPI. Actually, a real possibility of observing BLS from spin waves appeared after the invention of the multipass interferometer by Sandercock [66]. In this device light passes through the interferometer several times. Every time light passes the FPI the background is suppressed, therefore the contrast increases by many orders of magnitude. The essential improvement of the system has been done later with the introduction of a tandem interferometer, which contains two

multipass interferometers mountained on the same mechanical driver [67]. This increases the FSR of the spectrometer without reducing the resolution.

Since in BLS experiments the intensity of the optical signal to be detected is very small, photon-counting systems are widely used as detectors. These consist of a photomultiplier with extremely low dark noise rate (ITT FW130 and EMI 9863 photomultipliers are very popular), a fast-rise-time preamplifier, a wide-band amplifier, a pulse-height analyser with discriminator and a counter. The dark noise of the photomultiplier (that is the signal produced in the absence of input light) represents the lowest intensity of the detectable signal. Therefore, it is very important to reduce the dark current, and considerable efforts have been made to do so. Electrons thermally emitted by the photocathode account for an essential part of the dark current. This makes it possible to reduce drastically the dark current by cooling the photomultiplier. In the ITT FW130 photomultiplier, for example, the dark-noise rate is about 1 count s^{-1} at 240 K.

The Brillouin spectra of most magnetic systems require several hours of data accumulation time for a significant signal-to-noise ratio. On the other hand, the mirror alignment in multipass operation is very critical. For these reasons the multiscan procedure is used, when data from each rapid scan are accumulated in a computer or in a multichannel analyser. At the same time an active stabilization of the interferometer is performed. This makes use of a prominent line (e.g. the Rayleigh line) to control the mirror spacing and to optimize the mirror alignment. For details, see [67] and references therein. All these tasks may be completed by special electronic equipment [68] or by computer software and hardware [69].

In some particular cases the BLS line is powerful enough to be used for FPI stabilization. In this instance the BLS intensity can be measured continuously as a function of an external parameter, i.e. the applied field [70]. For continuous measurement the displacement of the movable mirror of the FPI is reduced in amplitude to cause the interferometer to pass only the satellite. In this regime, the FPI in fact serves as an extremely-narrow-band tunable high-contrast filter of the shifted frequency. The number of photons fed to a photomultiplier during one FPI scan is counted. It is proportional to the BLS intensity.

For many applications (e.g. for measuring weak interlayer coupling in magnetic multilayers, see section 4) the precise determination of the BLS line position is necessary. For this purpose a method of self-correlating transformation, proposed in [71], can be applied. In this approach the correlator $h(\nu)$ should be calculated:

$$h(\nu) = \int f(\nu') f_0(\nu' - \nu)\, d\nu' \tag{34}$$

where $f(\nu)$ is the measured peak and $f_0(\nu)$ is the apparatus function. Calculation of the real apparatus function for a multipass Fabry–Pérot interferometer is a complicated task, because the active stabilization system continuously changes the alignment of the mirrors. But the powerful peak corresponding to elastic scattering or even BLS from the surface mode provides a perfectly measured apparatus function in every spectrum. It can be applied for calculation in equation (34). Unlike $f(\nu)$ the correlator $h(\nu)$ is a smooth, symmetrical function. Its maximum shows the position of the centre of the measured peak. It is possible to find the position of the peak centre with an accuracy much better than the width of the peak, namely (0.1–0.2) GHz. The reliability of this method has been tested by comparison of the data obtained for the Stokes and anti-Stokes peaks of BLS from phonons and magnons in single films [71].

5. Two-dimensional effects in thin films

Over the last decade impressive investigations of spin waves in magnetic films have been performed by BLS. The existence of the surface mode and standing modes was confirmed experimentally and their properties and mutual interaction were studied. The frequencies of the spin waves depend on the saturation magnetization M_0, the exchange constant A, the magnetic volume and the surface anisotropy constants K_V and K_S, as well as other magnetic parameters of the film. Measured by light scattering, they can be used for gathering information about magnetic systems under investigation. The relative intensities of the different peaks in BLS spectra, corresponding to different scattering processes, also provide important information. Magnetic properties of thin films as well as characteristics of spin waves in them, investigated by BLS, are reviewed in [5, 4].

Recent development of the surface fabrication and analysis techniques enabled production of magnetic films with thicknesses of few monolayers. Such films demonstrate unique magnetic behaviour: surface anisotropy, enormous two-dimensional thermal fluctuation and disappearance of magnetic order, 'dead' magnetic layers and many others. These peculiar properties of thin films, studied by light scattering are the subject of this section.

Over the past decades magnetic properties of low-dimensional magnets have been thoroughly investigated by different experimental and theoretical methods. Many interesting phenomena existing in such systems were predicted theoretically, including a special kind of topological excitations and unusual phase transitions [72]. However, it was understood that the so-called 'quasi-two-dimensional' systems, i.e. bulk crystals consisting of magnetic layers, separated from each other by a large number of non-magnetic layers, always have small three-dimensional interactions which disturb low-dimensional effects dramatically. Therefore, from that point of view thin magnetic films or magnetic monolayers should be much closer to two-dimensional objects considered by theories.

According to the theorem of Mermin and Wagner a ferromagnetic ground state cannot exist at finite temperatures in an isotropic two-dimensional Heisenberg ferromagnet with short-range interaction [73]. This phenomenon is closely connected with the details of the spectrum of spin waves existing in such a system, since the long-range order is destroyed by the gapless spin waves with small wave vectors. There exists, however, experimental evidence of the long-range order in several two-dimensional systems (see e.g. [74]). Although the existence of magnetic uniaxial anisotropies can lead to stable two-dimensional ordering [75], it has been argued that magnetic-dipolar interactions play an important role in the processes [76]. On the other hand, both anisotropies and magnetic-dipolar interactions affect the spin-wave spectrum and can be extracted from the measured values of spin-wave frequencies. Therefore, it is very important and informative to investigate the spin-wave spectrum in two-dimensional systems.

The observation of the BLS from spin waves in 1 ML Co film on Cu(100) was reported in [77]. To prevent contamination the sample was coated with a 30 Å thick Cu film. It was thoroughly checked that the coating does not change the magnetic properties of the sample. The BLS experiments were performed at room temperature. From the BLS spectra the frequencies of the spin waves with wave vector $k_{||} = 1.73 \times 10^5$ cm^{-1} were determined. As mentioned in the previous sections, the exchange contribution to spin-wave frequency for such a small wavevector is negligible. Therefore, in fact it was the gap in the spin-wave spectrum (i.e. the spin-wave frequency at $k_{||} \to 0$, which is considered by the theories) that was measured.

Figure 9 shows the field dependence of the magnon energy (which is equal to $h\nu$, where ν is the spin-wave frequency), determined from BLS. The magnetic field is applied in the

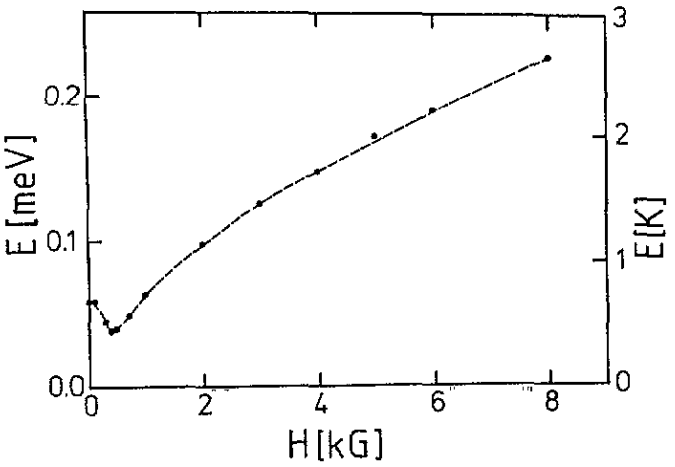

Figure 9. Magnetic field dependence of the magnon energy, determined from BLS spectra. The dashed line through the data points is a guide to the eye. The energy of 0.1 meV corresponds to the spin-wave frequency of 24.2 GHz (from [77]).

plane of the film along a [001] direction. The minimum of the curve in figure 9 occurs at $H = 400$ Oe. This is due to the fact that the [001] direction is not an easy direction for the in-plane magnetization. The hysteresis measurements confirm that the [001] direction is a hard axis for 1 ML Co on Cu(100). Using values of the gap in the spin-wave spectrum obtained from the BLS experiments and taking into account the magnetic-dipole interaction, the authors of [77] calculated the temperature dependence of the layer magnetization. It decreased very steeply with temperature. In contrast, the measured $M(T)$ dependence obtained on the same sample by means of magneto-optical Kerr magnetometry was almost constant up to 380 K. This is not surprising, because the sample under investigation had a large uniaxial in-plane anisotropy, which was experimentally found to play an important role for the stabilization of the magnetic order in quasi-two-dimensional magnetic crystals [78]. However, the existence of such an anisotropy was not taken into account in the calculations, used in [77].

The great influence of the magnetic anisotropies on magnetic order in thin films was confirmed by the detailed experimental study of better quality Co films on Cu(100). The investigation showed that at room temperature ferromagnetic long-range order exists only for the thicknesses more than $d_c = 1.6$ ML [57]. By means of BLS the spin-wave frequency as a function of the applied magnetic field was measured. By applying the external field along the magnetic hard axis, one can probe the magnetic anisotropies by studying the rotation of the magnetization with increasing field into the direction of the applied field via the corresponding change in the spin-wave frequency. The BLS experiments reported in [57] revealed the absence of the uniaxial in-plane anisotropy and the presence of the surface out-of-plane anisotropy. The energy contribution E_{an} due to anisotropies in this case is written as follows:

$$E_{an} = \frac{1}{4}\left(K_V^{\parallel} + \frac{2}{d}K_S^{\parallel}\right)\sin^2 2\phi \sin^4\theta + \frac{2}{d}K_S^{\perp}\sin^2\theta \tag{35}$$

where $K_V^{\parallel}$ and $K_S^{\parallel}$ are the in-plane volume and surface anisotropy constants of fourfold symmetry, and $K_S^{\perp}$ is the out-of-plane surface anisotropy constant. In figure 10 the total

fourfold in-plane anisotropy $K_{\text{in-plane}} = K_V^{\parallel} + 2K_S^{\parallel}/d$ and the out-of-plane anisotropy $K_S^{\perp}$ are plotted as a function of the Co thickness for the films with and without a 2 ML Cu overlayer. The value of $K_S^{\perp}$ is constant for $d > d_c$ within experimental error, while the behaviour of $K_{\text{in-plane}}$ permits one to distinguish between $K_V^{\parallel}$ and $K_S^{\parallel}$. These values cancel each other at d_c^* which corresponds to the critical thickness d_c of the existence of the ferromagnetic order. This attests to the fact that the symmetry-breaking interaction for the stabilization of ferromagnetic order in Co(100) films at room temperature is indeed given by the magnetic in-plane anisotropy contribution.

Playing an important role for the ferromagnetic order stabilization, surface anisotropy, however, is itself of special interest. This field has a large application potential in connection with the so-called 'perpendicular memory' [79]. BLS experiments appear to be a very useful technique to examine surface anisotropy effects. Besides the systems already mentioned, Co on a vicinal Cu(1113) plane [57], Fe(110) on W(110) [80] and Fe(100) on Ag(100) [81] have been investigated.

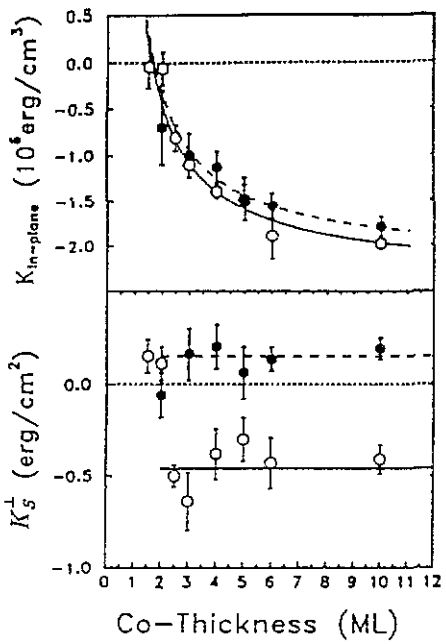

Figure 10. Obtained in-plane (upper part) and out-of-plane (lower part) anisotropy constants as a function of the Co layer thickness (in ML) for Co/Cu(001) without (open circles) and with (solid circles) a 2 ML Cu overlayer. A fit of the theory according to equation (35) is shown for Co/Cu (solid line) and for Cu/Co/Cu (dashed line) (from [57]).

Very interesting studies were performed on FCC Fe(100) grown on Cu(100) [82, 83], which we describe in more detail. The samples used in the study were grown by MBE in ultra-high vacuum (10^{-10} Torr) on single-crystal Cu(001). They contained 3 ML of Fe covered by a Cu overlayer. The BLS experiments were performed at room temperature with the help of a six-pass (4+2) tandem Fabry–Pérot interferometer. 200 mW of light polarized in the scattering plane (Ar^+ laser, $\lambda = 514.5$ nm) was focused onto the sample surface and 180° back-scattered light, polarized perpendicular to the scattering plane, was analysed

with the interferometer. The angle of incidence of the light was 45°. A magnetic field was applied in the plane of the sample and perpendicular to the scattering plane. Thus, scattering from the surface spin waves propagating along the sample surface perpendicular to the applied field was observed. The observed representative BLS spectrum is shown in figure 11. There is a small asymmetry between intensities of Stokes and anti-Stokes peaks which reversed with the reversal of the magnetic field, that has been already observed and discussed before [46]. Figure 12 presents the surface spin-wave frequency as a function of the applied in-plane field. The frequency was found to be independent of the direction of the magnetic field in the sample plane. Both these findings lead to the conclusion that at zero applied field the magnetization vector M_0 is aligned perpendicular to the sample plane. This was assumed to be due to large out-of-plane anisotropies. In this case the anisotropy energy can be written as

$$E_{an} = -K_{S1}^{\perp} \sin^2 \alpha - K_{S2}^{\perp} \sin^4 \alpha \tag{36}$$

where α is the angle between M_0 and the sample plane. Both the critical field H_c

$$H_c = -(4\pi M_0)_{eff} = \frac{2K_{S1}^{\perp}}{M_0} - 4\pi M_0 \tag{37}$$

and the spin-wave frequency at zero field is connected with $K_{S1}^{\perp}$ and $K_{S2}^{\perp}$. The solid line in figure 12 was calculated using an approach which is similar to the one of Cochran and Dutcher [47]. By varying $K_{S1}^{\perp}$ and $K_{S2}^{\perp}$ the best fit was obtained and the fitted values of $K_{S1}^{\perp}$ and $K_{S2}^{\perp}$ were determined.

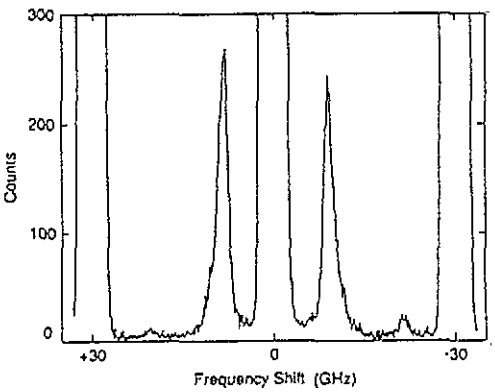

Figure 11. BLS spectrum for surface spin waves in 60 ML Cu/3 ML Fe/Cu(001) for an applied field of $H = 5.81$ kOe. The small peaks occurring at ± 21.4 GHz are ghosts from the second-order Rayleigh peaks (from [82]).

The magnetic field dependence of the scattering intensity is presented in figure 13. The fitting curve was calculated using the magnetic parameters determined from the frequency measurements (figure 12). A free parameter (the total y-axis scale) was used to fit experimental data in figure 13. The agreement between the data and the calculation is almost perfect. A dramatic increase of the scattering intensity near H_c can be understood as follows. At this point the effective field acting on the magnetization drops to zero.

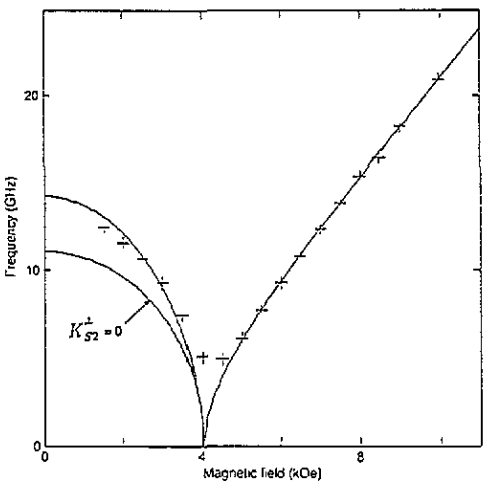

Figure 12. Magnetic field dependence of the surface mode frequency for the 60ML Cu/3ML Fe/Cu(001) sample. The crosses are measured data points. The solid curve which passes through the data points is the result of a fit according to equation (36). The curve calculated with $K_{S2}^{\perp}=0$ is also indicated (from [83]).

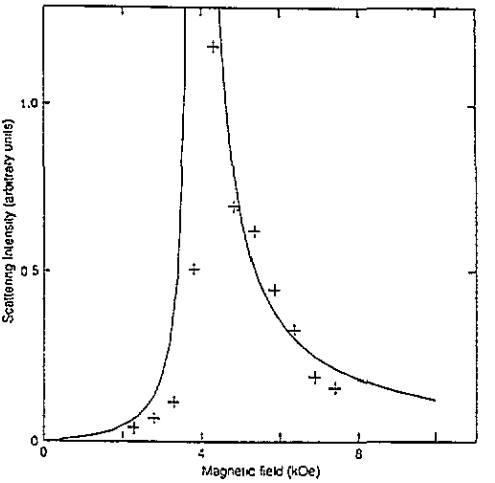

Figure 13. Magnetic field dependence of the scattering intensity for the 60ML Cu/3ML Fe/Cu(001) sample. The crosses are measured data points. The solid curve which passes through the data points is the result of calculations. Only the first-order magneto-optic constant was used in the calculation of the scattering intensity (from [83]).

This causes an increase of the amplitude of the fluctuating precessing magnetization. The relatively large transverse magnetization components give rise to the large light scattering intensity. The same phenomenon could be explained in terms of statistics of spin waves. Due to the sharp decrease of the frequencies of spin waves near H_c their occupation numbers n_ω increase dramatically and therefore the light scattering intensity which is proportional to n_ω or $n_\omega + 1$ rises. In this connection we notice that the authors of [82, 83] do not discuss two-dimensional fluctuation effects in their films. It was, however, experimentally found that such effects are of special importance in the presence of a spin orientation transition and can result in the renormalization of the critical field H_c [78]. In this case the relation between the measured critical field and the spin-wave frequency at zero field is changed.

We also dwell on the experiments on an (001) Fe whisker [84], where an elegant experimental study of the surface anisotropy was carried out. The whiskers were cleaned in an ultra-high vacuum and covered with 15 ML of gold or with a layer consisting of 15 ML of silver and then 30 ML of gold. This was done to protect the whisker surface from oxidation and to investigate the influence of the overlayer material on the value of surface anisotropy. The scattering geometry was similar to that used in [83]. It turned out to be possible to determine the value of the surface anisotropy even for very thick films (or whiskers) by measuring the dependence of the surface-mode frequency on the in-plane wavevector. In this case, of course, high-accuracy frequency measurements are needed, because the influence of the surface anisotropy on the mode frequency in the case of whiskers is not so essential as in the case of thin films.

A typical BLS spectrum obtained on an Fe whisker for an applied field of 5.033 kOe is shown in figure 14. The spectrum consists of a single peak (surface mode) on one side of the spectrum and continuous bands (bulk modes) on both sides of the spectrum. As was explained in section 3, the surface mode manifests itself only on one side of the spectrum

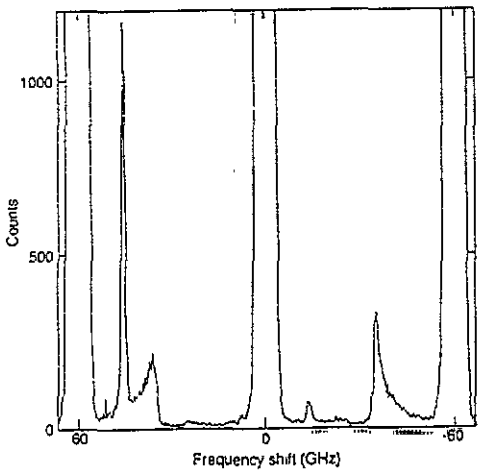

Figure 14. BLS spectrum for 15 ML Au/Fe(001) whisker with an applied field of $H = 5.003$ kOe. The small peak that occurs at -14 GHz is a ghost peak (from [84]).

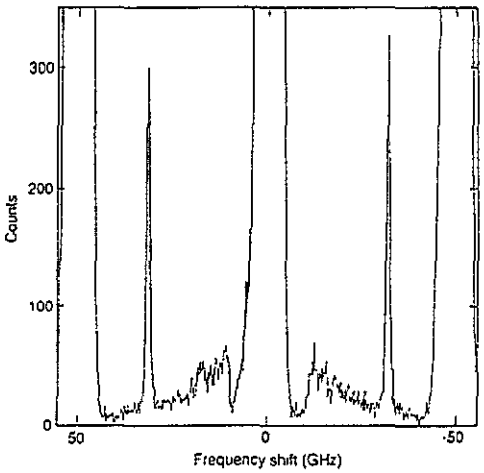

Figure 15. BLS spectrum for 15 ML Au/Fe(001) whisker in zero applied field. The domain wall is at the centre of the focused laser spot (from [84]).

for thick uniformly magnetized samples and it can be moved from one side to the other side by reversing the direction of the magnetization [10]. The magnetization reversal can be easily done by moving the domain wall across the width of the whisker by a small change in the applied field. The domain wall can be also 'parked' on the laser spot. Since the domain wall is much narrower than the laser light spot, both domains are observed at the same time and the surface-mode peak appears on both sides of the spectrum. The corresponding BLS spectrum is shown in figure 15. A judicious choice of small FSR permits the observation of both the up-shifted and down-shifted surface-mode peaks on the same side of the spectrum, as shown in figure 16. This particular feature is extremely useful for high-precision measurements of small frequency shifts in a zero applied field, because the two peaks shift in opposite directions, when the frequency of the surface mode changes.

A change in the angle of incidence of light θ (measured with respect to the sample normal) from $\theta = 32°$ to $\theta = 68°$ results in a shift in the frequency of the surface mode of 0.293 GHz for the 15 ML Au/Fe(001) whisker and 0.221 GHz for the 30 ML Au/15 ML Ag/Fe(001) whisker. The comparison of the calculated shift in the surface-mode frequency with the observed one provided an unambiguous determination of the value of the surface out-of-plane anisotropy $K_{S1}^{\perp}$. The value of $K_{S1}^{\perp} = 0.54 \pm 0.05$ erg cm^{-2} was obtained for 15 ML Au/Fe(001) whisker and the value of $K_{S1}^{\perp} = 0.79 \pm 0.05$ erg cm^{-2} was obtained for 30 ML Au/15 ML Ag/Fe(001) whisker. These values are in good agreement with the values of K_S for ultra-thin iron films [85]. Such an agreement shows that the surface anisotropy is not unique for epitaxially grown thin films but a consequence of the abrupt change in symmetry at the surface as proposed by Gay and Richter [86].

We have already mentioned that BLS experiments are performed mainly on monocrystalline samples. This is due to the fact that in polycrystalline samples the BLS spectra are broadened, the broadening being caused by averaging the anisotropy-axis orientation. However, there are several publications on this subject. Light scattering in polycrystalline CoPt and CoNiPt alloys films was studied in [87, 88]. In both cases BLS from the surface and standing bulk spin waves was observed. From the values of the both mode frequencies

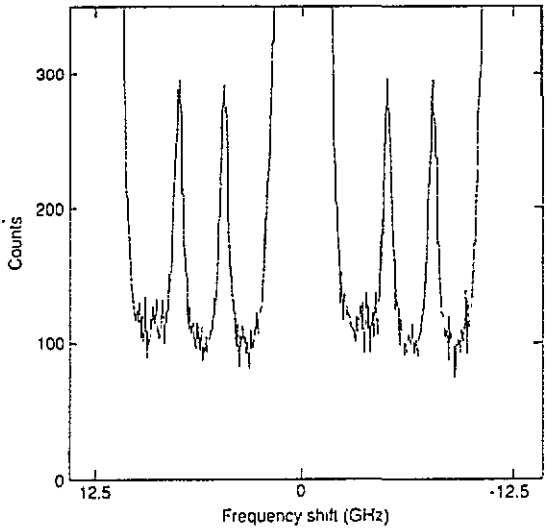

Figure 16. BLS spectrum for 15 ML Au/Fe(001) whisker in zero applied field using a single interferometer and a small free spectral range (12.5 GHz). The domain wall is at the centre of the focused laser spot (from [84]).

and their field dependences the exchange stiffness constants were determined. The spectra were remarkably broadened because of the magnetic inhomogeneity due to the grains in the film. The BLS from surface and standing bulk spin waves in FeSi (2.6 wt% of Si) sputtered films were reported in [89]. From the comparison of the measured frequencies with the theoretical calculation the magnetic constants of the film were determined. The exchange stiffness constant was found to be about 50% of the Fe film.

6. Light scattering in layered magnetic systems

It was shown in the previous section that the light-scattering experiments provided a lot of information about spin waves in magnetic films, which in their turn clarify interesting physical phenomena, such as surface anisotropy and two-dimensional magnetic fluctuations. However, the light scattering from spin waves in layered systems is enormously more peculiar and diverse.

Layered magnetic systems have been a subject of growing interest for the last few decades. This is stimulated, to some extent, by the expectation that layering provides a new possibility of tayloring magnetic properties. This expectation was partly justified by the discovery of antiferromagnetic coupling between two magnetic layers across a non-magnetic spacer [90] and a giant magnetoresistance effect [91,92]. The latter takes place, for example, when the antiferromagnetically aligned magnetizations of the magnetic films are aligned to be parallel by applied magnetic field.

It was explained in section 2 that there are two basic contributions to the interlayer coupling, namely magnetic-dipolar and exchange interactions. The former is of long-range nature and it was investigated theoretically and experimentally. It was shown that in layered systems the dipolar coupling modifies the spectrum of the spin-wave modes [4], but it cannot result in any measurable antiferromagnetic- or ferromagnetic-type coupling between the

static magnetizations of different films [93]. However, very recent calculations show that the dipolar interaction together with interface roughness, existing in real systems, provides a biquadratic coupling, which favours the perpendicular orientation of the static magnetization [94]. The experimental verification of the latter prediction could be done in light-scattering experiments, if detailed information about the interface morphology were available.

The exchange coupling is a contact one, it occurs by the direct hybridization of spin orbitals (direct exchange) or is transferred through a non–magnetic substance (the so-called RKKY-type coupling) [95]. The latter has long-range nature, and could be roughly described as follows. The coupling between two magnetic moments arises from the spin polarization of the conducting electron gas. This polarization has oscillation behaviour and changes its sign, i.e. the interaction is ferro- or antiferromagnetic with a given period and decays in accordance with a power law for long distances between interacting moments.

In this section we consider an experimental investigation of spin waves in layered magnetic systems by means of BLS. The most important point in these studies is the fact that the frequencies of spin waves in layered systems depend on the coupling between different magnetic layers. Therefore, measuring these frequencies by BLS one can obtain information about the type and the strength of coupling in such systems. Since magnetic bilayers (layered systems consisting of two magnetic films) represent the simplest arrangement for the study of the interlayer coupling, the majority of these BLS experiments was performed on bilayers. Therefore, we review these experiments first. More complicated systems, multilayers (layered system consisting of many, usually dozens, of magnetic films), are considered separately.

6.1. Exchange coupling in bilayers

In real layered magnetic systems a large direct ferromagnetic-type exchange for a relatively thin non–magnetic spacer is often observed. This occurs due to magnetic 'bridges' in the spacer, i.e. direct contacts between two magnetic films. Recent achievements in growth methods make it possible to avoid 'bridges' in the best samples for spacer thicknesses more than 0.2–0.4 nm. Therefore, the interlayer exchange coupling observed in these circumstances is thought to be connected with carriers in non–magnetic spacers. The antiferromagnetic type of coupling across a non-magnetic spacer (which is obviously not connected with 'bridges') was discovered by means of BLS in the Fe/Cr/Fe system for Cr thicknesses around 0.8 nm [90]. This discovery was confirmed in [96]. Representative BLS spectra from [96] for 10 nm Fe/Cr/10 nm Fe samples and for a 20 nm Fe single layer are shown in figure 17. As was expected (see subsection 2.1), two spin-wave modes were detected by means of light scattering. The first one is the surface mode. Its frequency is independent of the spacer thickness and it can be used for the evaluation of the magnetic anisotropy field in Fe films. The second mode corresponds to the out-of-phase precession of magnetic moments in two Fe films and its frequency is sensitive to the interlayer exchange. Using the parameters obtained from the position of the surface-mode line, the position of the second mode line for vanishing interlayer exchange was predicted. It is marked in figure 17 by a dashed line. A clear frequency downshift of the second mode is pronounced for $d_{Cr} = 0.8$–1.2 nm. The fact that this mode is observed at a frequency which is lower than the value corresponding to zero interlayer coupling can only be interpreted as indicating that the exchange has become antiferromagnetic. For comparison the Fe/Au/Fe system was also studied in [90, 96]. In contrast to the Fe/Cr/Fe bilayer an essential (for $d_{Au} < 12$ nm) or slight frequency upshift was always observed for the exchange-sensitive mode of the Fe/Au/Fe system. It should be noted that the later investigations revealed the existence of AF coupling in Fe/Au/Fe layered systems [97]. However, this coupling is much weaker

than that for Fe/Cr/Fe, therefore it could not be detected in [90, 96]. Comparison of the observed frequencies with the results of the numerical calculations [26] enables one to obtain the dependence of the coupling strength on d_{Cr} and d_{Au}. This dependence is shown in figure 18, which is taken from [96].

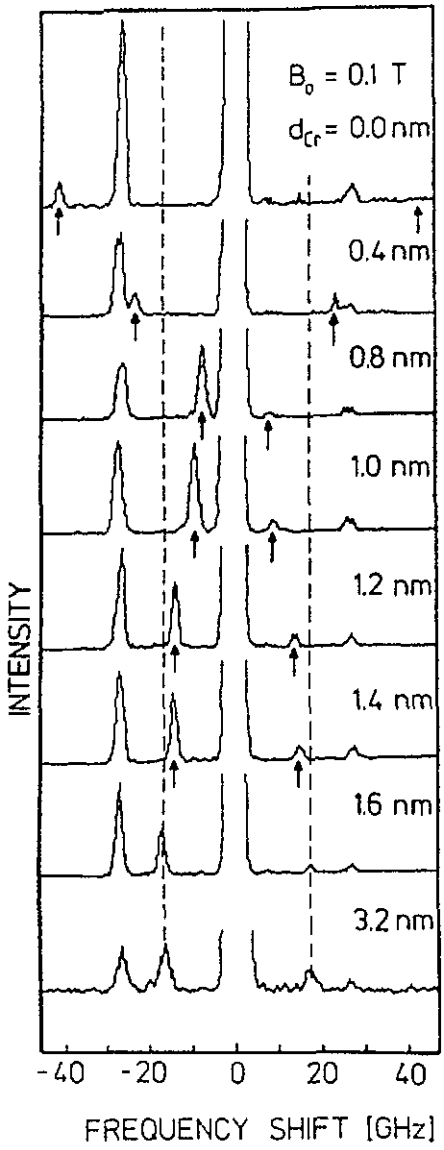

Figure 17. BLS spectra in a 10 nm Fe/Cr/10 nm Fe layered system with Cr thickness as indicated. The arrows point out the exchange-sensitive mode. The dashed line shows the position of this mode in the case of zero interlayer coupling (from [96]).

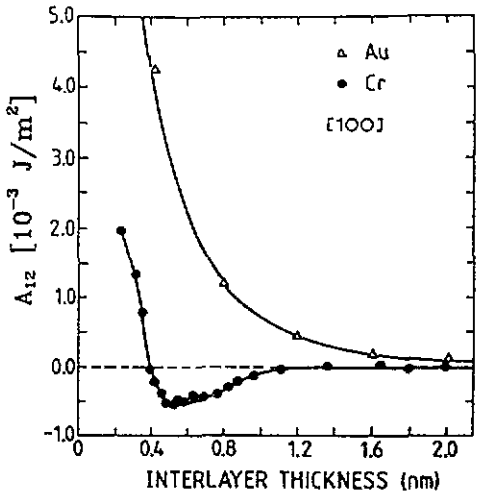

Figure 18. The interlayer coupling strength A_{12} as a function of the spacer thickness for 10 nm Fe/Cr/10 nm Fe and 10 nm Fe/Au/10 nm Fe. The negative sign of A_{12} corresponds to AF-type coupling (from [96]).

After the discovery of the AF-type coupling in the Fe/Cr/Fe system, BLS has been investigated in another layered system possessing this type of coupling, namely in Fe/Cu/Fe

grown on bulk silver [98]. Single magnetic layers Ag/Cu/Fe/Au and magnetic bilayers Ag/Fe/Cu/Fe/Au with thicknesses of individual layers from five to 20 monolayers (ML) were studied. The former were used for the determination of the magnetic properties of Fe layers (i.e. values of the magnetization, bulk and surface anisotropies); the latter were used for investigation of the interlayer exchange. For Cu thicknesses less than 9 ML the coupling between Fe films was found to be ferromagnetic; for thicknesses between 9 and 12 ML the coupling was found to be antiferromagnetic. In figure 19 a light-scattering spectrum for one of the bilayers (Ag/5 ML Fe/11.6 ML Cu/10.3 ML Fe/20 ML Au) at zero applied magnetic field is presented. It shows the slightly different frequencies which are observed for low-frequency Stokes and anti-Stokes lines. This difference is expected for magnetic bilayers having oppositely oriented magnetizations.

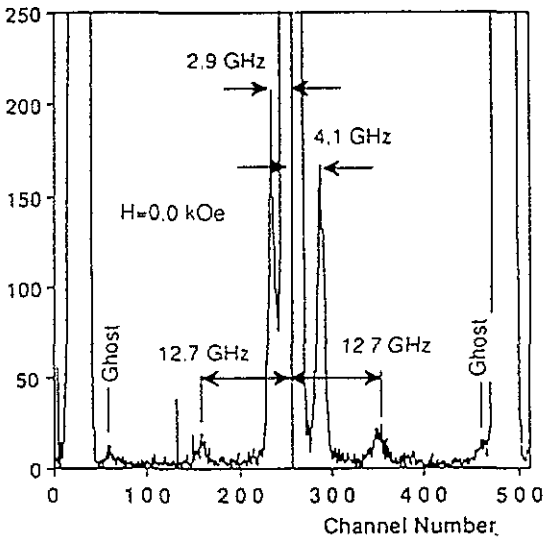

Figure 19. BLS spectrum for (Ag/5 ML Fe/11.6 ML Cu/10.3 ML Fe/20 ML Au) obtained in back-scattering configuration and at zero applied field. The free spectral range used was 30 GHz and 454 channels=60 GHz. The figure illustrates the slightly different frequencies that were observed for Stokes and anti-Stokes lines for one of the modes (from [98]).

After the observation of the AF-type coupling in these systems many other systems followed, and now this kind of coupling has been found in more than 20 systems, with Fe, Co, Ni or their alloys being magnetic layers [99].

However, it appeared to be very complicated to perform a detailed investigation of the interlayer coupling strength using samples with constant thickness of the films. Such study became particularly important after the appearance of a publication [100], where Fe/Cr/Fe and Co/Ru/Co multilayers were investigated by measuring the $M(H)$ magnetization curves. It was reported that a saturation field (i.e. the field to be applied to obtain a saturation of the total magnetization of the multilayer) reveals damping oscillations as a function of the non-magnetic spacer thickness. For the AF-type coupling the saturation field thought to be proportional to the coupling strength. However, the evaluation of the $M(H)$ curves did not give any information about the ferromagnetic-type coupling. Therefore, it was a challenge to the light-scattering technique to investigate thoroughly the coupling as a function of spacer thickness and to confirm its oscillating behaviour.

Introduction of samples with a wedge-type interlayer was a very important improvement of the method and it allowed a considerable increase of the accuracy of the measurements [101, 71]. The wedge-type sample has the advantage that the continuous range of spacer thicknesses can be studied on one sample with identical Fe films. This reduces the number

of samples to be prepared and at the same time tremendously increases the reliability of the study, since scattering due to unavoidable differences in the preparation conditions is suppressed. The slope of the Cr wedge in the examined samples was very small, of the order of 2 Å mm^{-1}; this corresponds to one atomic step per one millimetre. Actually, using light scattering one can examine spin waves in a layer system at the area of the focused probing laser beam (i.e. 100–50 μm). For the investigation of different d_{Cr} the beam is scanned across the sample.

It is clear that at least for a high enough applied field, when all regions of the wedge samples are saturated, the wedge geometry does not modify the magnetic behaviour of the films. This results from the fact that on the scale of 10 μm (mean free path of spin waves) the changes of the spacer thickness are negligible, therefore the frequency of spin waves is the same as for the sample with a constant thickness of spacer. In the case of an intermediate state, when the parts of the sample with a large AF-type coupling are not saturated whereas other parts of the sample are saturated, the situation is not so clear. Domain walls, created by such a micromagnetic arrangement, could produce magnetic-dipolar fields which, in their turn, could disturb spin-wave behaviour at other parts of the sample. However, detailed comparison of the results obtained on the wedge-type samples with the results obtained on the sample with constant thicknesses confirms the possibility of using the wedge-type samples for studies of interlayer coupling. Nowadays wedge-type layered systems are widely used not only in light-scattering investigations but also in magneto-optical magnetometry [71], magneto-optical Kerr microscopy [102] and in scanning electron microscopy [63].

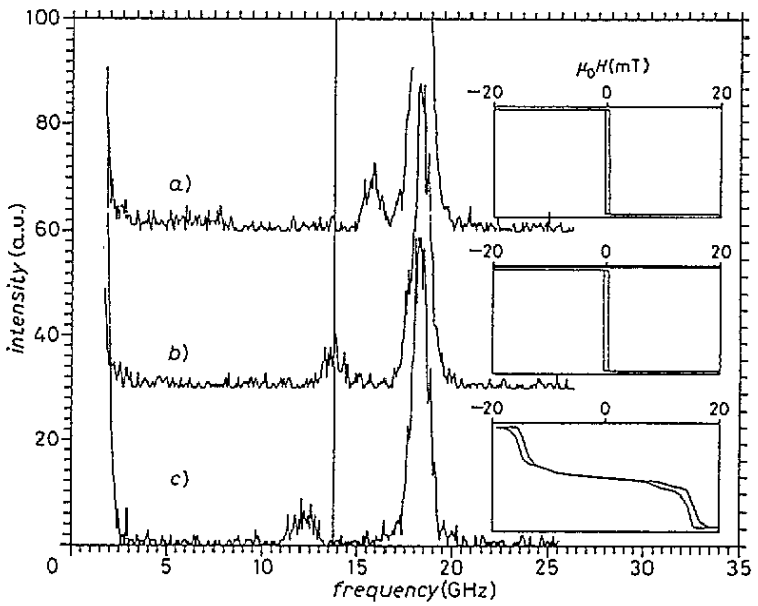

Figure 20. BLS spectra from spin waves in an Fe/Cr/Fe double layer for different thicknesses of Cr, measured at $H = 1.5$ kOe: (a) $d_{Cr} = 1.8$ nm, (b) $d_{Cr} = 2.2$ nm, (c) $d_{Cr} = 2.5$ nm. The intensive line of frequency 18.3 GHz corresponds to the surface mode. The vertical line shows the calculated position of the exchange-sensitive mode for zero coupling. The insets near the spectra present the $M(H)$ curves measured for the same d_{Cr} (from [71]).

A thorough study of the interlayer coupling in Fe/Cr/Fe bilayers was performed in [71, 103]. Figure 20, taken from [71], shows the light-scattering spectra for different values of d_{Cr} corresponding to the ferromagnetic, zero and antiferromagnetic coupling between Fe films. The insets placed near the spectra present $M(H)$ curves measured for the same d_{Cr}. Two spin-wave modes are distinctly seen. The first one is the surface mode of which the frequency is independent of the interlayer coupling. This was used to test the magnetic homogeneity of Fe films and to determine magnetic parameters of the sample, such as the saturation magnetization and anisotropy constants. In the experiments under discussion the surface-mode frequency was constant with an accuracy of 0.3%. The other mode is sensitive to the interlayer exchange. With the help of a fitting procedure [27] the coupling strength parameter A_{12} (see subsection 2.1) was calculated from its frequency.

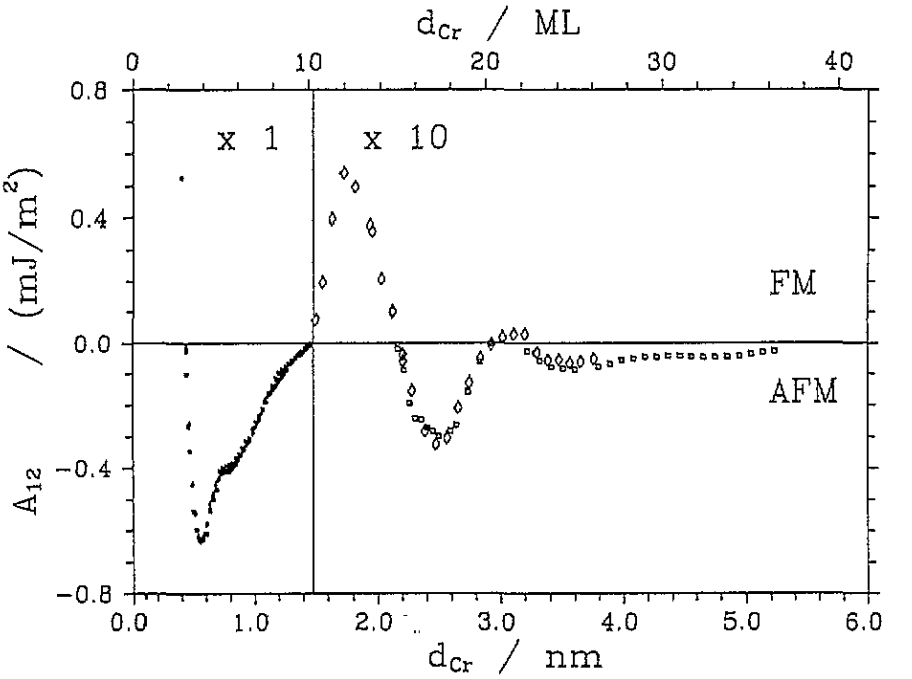

Figure 21. Interlayer constant A_{12} as a function of d_{Cr} at room temperature, obtained from BLS (◇) and $M(H)$ (□) measurements (from [71]).

Figure 21 shows the oscillating A_{12} dependence for Fe/Cr/Fe layered systems, obtained in [71]. In addition to the known region of AF-type coupling [90] the data reveal two other AF-type-coupling regions, separated by regions where the coupling is ferromagnetic. Thus, the BLS experiments not only confirm the oscillating behaviour of the interlayer coupling, reported in [100], but demonstrate that the coupling, in fact, does have an oscillating behaviour. The period of the oscillation obtained from these measurements is about 1.7 nm. Moreover, the $A_{12}(d_{Cr})$ curve in figure 21 also displays fine structure in the first AF region around $d_{Cr} = 0.8$ nm. This indicates the existence of further maxima of AF-type coupling within that range. From the theoretical point of view the oscillating coupling is connected with the topology of the Fermi surface of conducting electrons in the non-magnetic spacer,

the period d being equal:

$$d = \frac{\pi}{k_F^e} \tag{38}$$

where k_F^e is the extreme radius of the Fermi surface. Thus, from the known topology of the Fermi surface of Cr the theory predicts the existence of the second shorter period $d = 0.29$ nm [104, 105]. Very flat interfaces are a necessary precondition for its occurrence [104]. Actually, the data obtained from BLS on the Fe/Cr/Fe epitaxial system with improved interfaces due to a special electron-beam treatment apparently reveal short period oscillations [103] (see figure 22(a)). Final evidence came from samples grown on Fe whiskers [106], the quality of which was evidently attested to by the RHEED patterns. Figure 22(b) displays the dependence of the out-of-phase mode frequency, which reflects the $A_{12}(d_{Cr})$ coupling curve. The short-period oscillation has a larger amplitude, than in the case of the samples grown on GaAs substrates. Thus, these studies experimentally confirmed the correlation between the amplitude of the short-period oscillation and the quality of the interfaces.

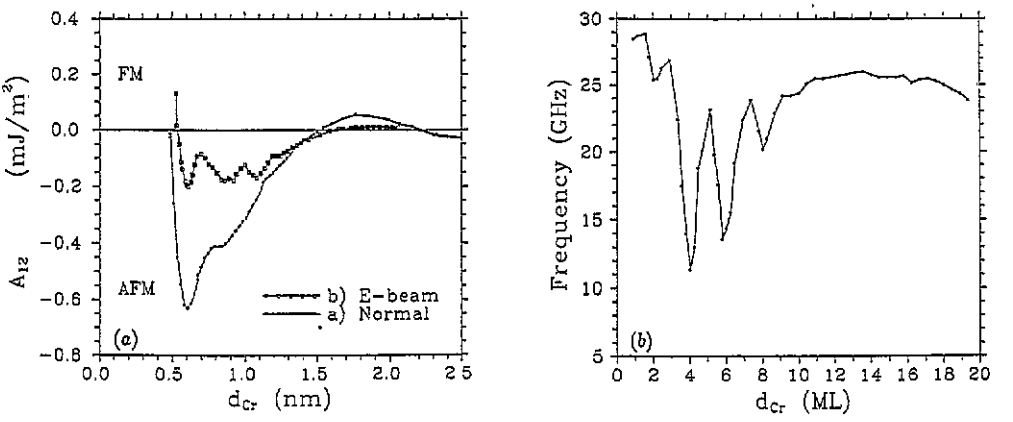

Figure 22. $A_{12}(d_{Cr})$ dependence for Fe/Cr/Fe layered systems (a) grown on GaAs with and without electron-beam treatment, (b) grown on an Fe whisker. In (b) the exchange-sensitive-mode frequency is displayed, which is approximately proportional to A_{12} (from [106]).

An investigation of exchange coupling in an Fe-whisker based Fe/Cr/Fe layered system has been reported in [62]. A representative BLS spectrum for an Fe whisker/11ML Cr/20ML Fe/20ML Au sample is shown in figure 23. The peak labelled TF is supposed to be connected with BLS scattering from the spin-wave mode of the thin Fe layer, which is sensitive to interlayer coupling, whereas the peak labelled SM corresponds to the whisker surface mode. Their frequencies versus applied magnetic field for the Fe whisker/8 ML Cr/20 ML Fe/20 ML Au sample are shown in figure 24. The magnetic-field variation of the frequency of the thin-film mode is characterized by the presence of two cusps which occur at fields labelled H_1 and H_2 in figure 24. The existence of two critical points in the field dependence indicates the presence of the biquadratic term in the interlayer coupling which has been discovered in the Fe/Cr/Fe layered system by domain observation and $M(H)$ measurements [102]. From the values of these fields the bilinear and biquadratic interlayer exchange parameters

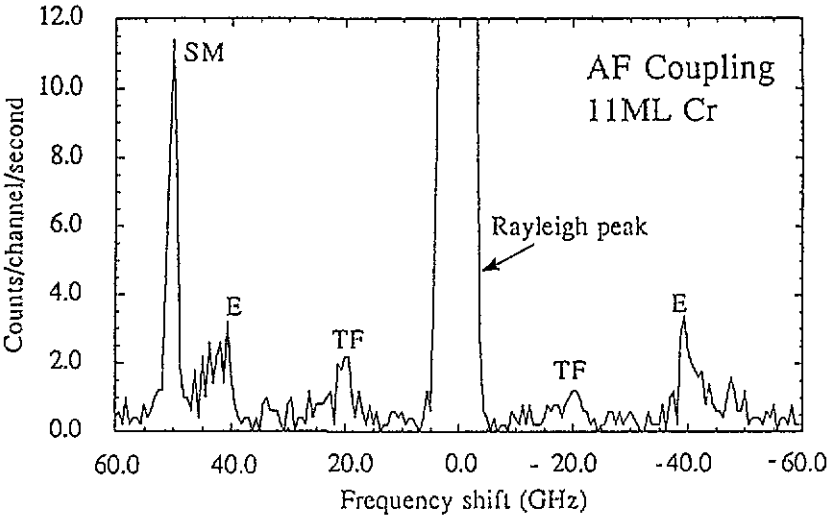

Figure 23. BLS spectrum for an AF-coupled Fe whisker/11ML Cr/20ML Fe/20ML Au structure at applied field 6 kOe. SM is the bulk surface mode; TF the exchange-sensitive thin film modes; E the bulk manifold edges (from [62]).

were obtained. Both parameters exhibited a short-period-oscillation dependence on the Cr interlayer thickness with a period of about 0.29 nm.

The dependence of the spin-wave frequencies in the Fe/Cr/Fe layered system on applied magnetic field and on in-plane wavevector $\mathbf{k}_{\parallel}$ was examined in [107]. A careful match between the features of the magnetization curves and BLS data gave accurate values of the magnetic parameters (including the AF-type coupling strength) for the layered system under investigation.

By means of BLS the interlayer coupling was also investigated in the Fe/Al/Fe layered system [97]. This study is of special interest insofar as Al does not belong to the transition metals and does not possess d electrons. Nevertheless, the experiments revealed AF-type bilinear and biquadratic interlayer coupling, which oscillates as a function of the Al spacer thickness. The period of the oscillation is about 1.9 nm which is close to that observed in Fe/Cr/Fe layered systems. The short-period oscillation was not observed in Fe/Al/Fe bilayers. This fact is in agreement with the poor quality of the interfaces, following from the RHEED patterns [97].

Besides BLS other experimental techniques, such as magneto-optical Kerr magnetometry, ferromagnetic resonance and scanning electron microscopy with polarization analysis were applied to the studies of the interlayer coupling. They revealed short-period and long-period oscillations of the coupling in the layered magnetic systems with different spacer materials [99]. This fact is a strong support for an RKKY-type mechanism of the coupling.

6.2. Spin waves and interlayer coupling in multilayers

As compared to bilayers, multilayer systems which contain many successive layers of magnetic or non-magnetic materials have not been investigated in such detail. This is caused by two factors: firstly, the theory of spin-wave modes in multilayers is more complicated than that for bilayers; secondly, it is a much more difficult problem to produce good-quality multilayers and to perform BLS experiments on them. However, several investigations of magnetic multilayers by means of light scattering have been reported recently.

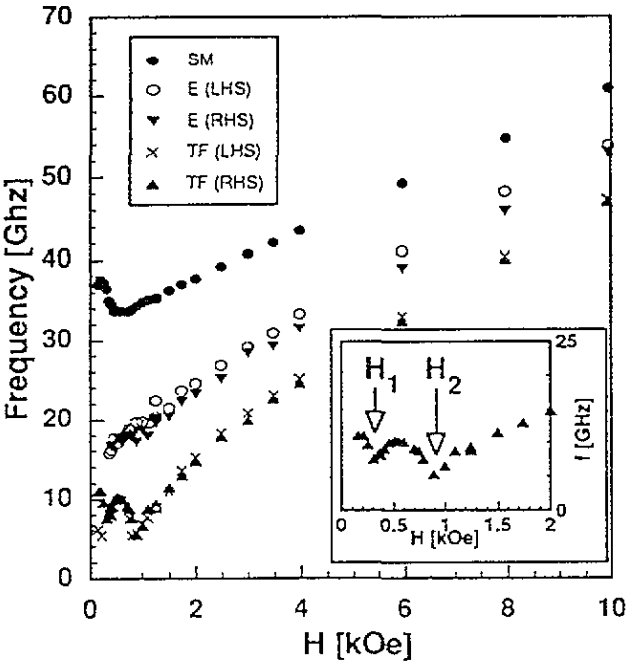

Figure 24. BLS peak frequency versus applied magnetic field for the Fe whisker/8 ML Cr/20 ML Fe/20 ML Au structure. The inset shows details of the low-field region. The presence of the cusps at the fields H_1 and H_2 is a signature of the AF-type coupling between the Fe thin film and the bulk whisker (from [62]).

As was shown in section 2, besides the surface mode spin wave a band of bulk excitations forms in a magnetic multilayer. This band arises due to dipolar coupling between spin waves in different layers even without direct magnetic interaction between adjacent layers. The experimental evidence for the existence of such a band by means of BLS was given in [108].

Similar to the situation in bilayers the exchange coupling between magnetic layers modifies the spectrum of spin-wave modes in multilayers. The experimental evidence for such a modification was obtained by Hillebrands *et al* [109]. Sputtered Co/Pd multilayers with eight and 30 periods were grown, the number of atomic layers n in each Co and Pd layer being the same. Different samples with variation of n between one and 32 were prepared. It was assumed that the interlayer coupling should increase with decreasing d_{Pd}. The BLS experiments were performed in an external field of $H = 5$ kOe, which was applied parallel to the layer planes and perpendicular to the scattering plane. The applied field was large enough to saturate the samples. The BLS spectra of a series of Co/Pd multilayer samples are shown in figure 25. For the sample with the thickest layer, $n = 32$, a spectrum typical of collective dipolar excitations is observed. The mode character was determined by typical Stokes–anti-Stokes asymmetry. The open arrows in figure 25 indicate the surface modes, whereas the solid arrows indicate the bulk bands. With decreasing layer thickness (increasing interlayer exchange) the surface mode remains essentially unchanged in frequency. However, the frequency of the bulk mode, sensitive to the interlayer coupling, increases with decreasing n and rises above that of the surface mode.

This observed phenomenon is in qualitative agreement with the theory [37, 28].

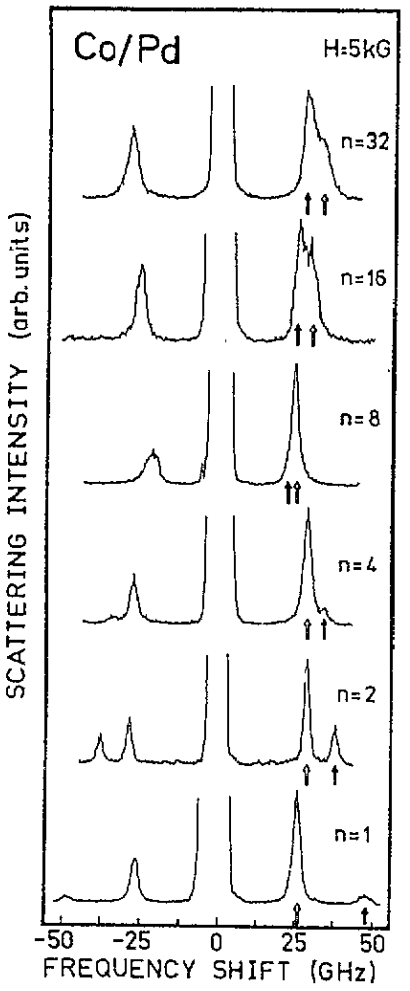

Figure 25. BLS spectra of $(Co/Pd)_{30}$ multilayers at $H = 5$ kOe. The number of atomic layers per magnetic and non-magnetic film is indicated by n. The open arrows denote modes which are predominately surface modes in character, the solid arrows those which are mainly bulk modes in character (from [109]).

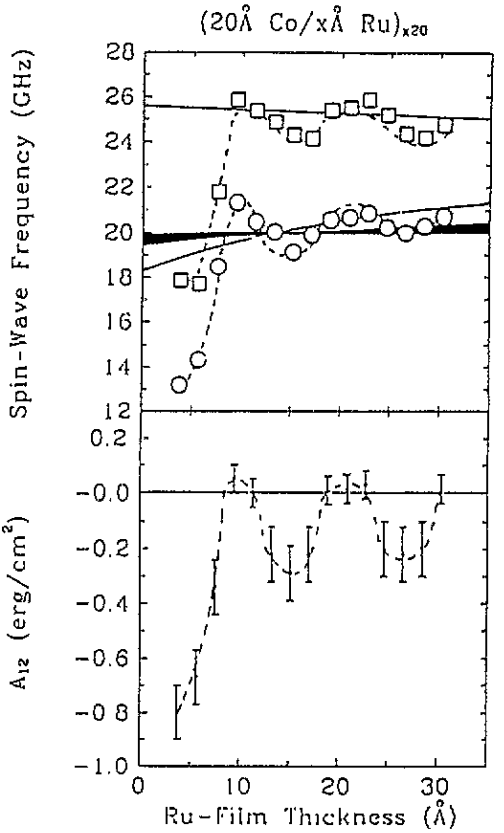

Figure 26. Upper part: frequency of the surface mode (squares) and the centre of the bulk modes (circles) as a function of the Ru layer thickness measured at $H = 3$ kOe. For comparison, the calculated frequencies for zero interlayer exchange are shown as full lines. Lower part: determined values of the interlayer exchange constant, A_{12}, as a function of the Ru layer thickness (from [110]).

Unfortunately, a quantitative comparison was not made, since the numerical instabilities limited the maximum number of magnetic layers for which spin-wave frequencies can be calculated to $N = 10$. On the other hand, the samples with eight periods only exhibited dipolar modes and did not show evidence of exchange-dominated collective modes. The reason for this is not yet clear.

It was shown in recent publications that BLS is applicable to the determination of the interlayer coupling strength in multilayered structures [110, 111]. The experiments were performed on sputtered Co/Ru and permalloy/Ru multilayers at a relatively low applied magnetic field. In this case the samples with the AF-type coupling were not saturated and

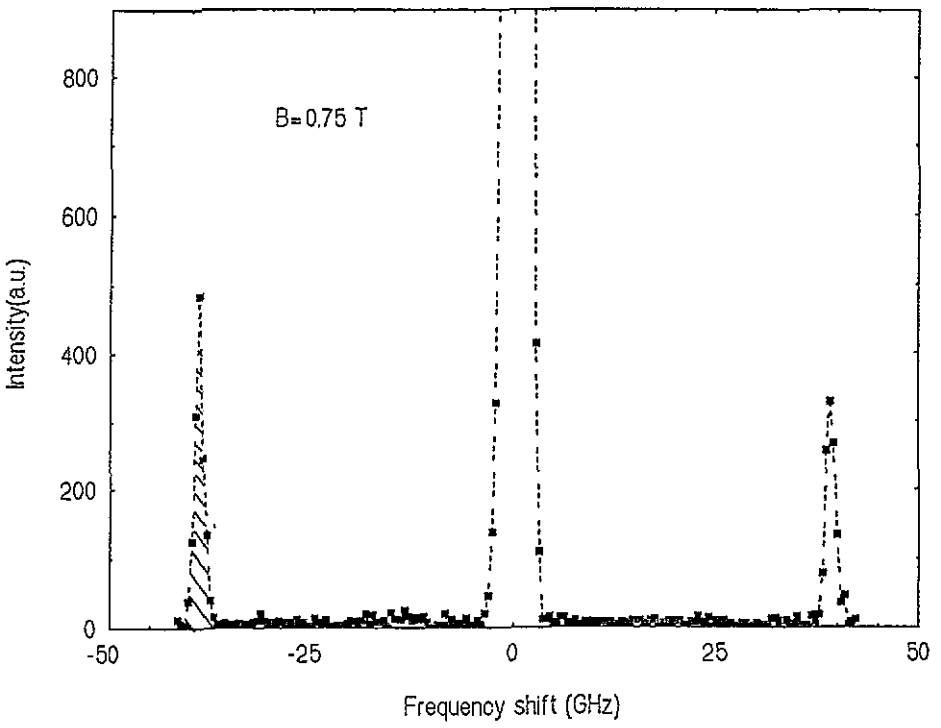

Figure 27. BLS spectrum from pumped spin waves in the Fe/Cr/Fe bilayer. The intensity of the shaded peak is used to record the resonance line. Note the difference in intensity of the Stokes and anti-Stokes peaks (from [119]).

there existed a canting angle between the magnetization of neighbouring magnetic layers, which was determined by the ratio between the applied field and the coupling strength. The frequency of the surface mode does not depend on the interlayer coupling directly, but it depends on the canting angle. Therefore, in such a situation not only the position of the bulk spin-wave band, but also the frequency of the surface mode is sensitive to the interlayer coupling and could be used for its determination.

The upper part of figure 26 shows the frequency of the surface mode and the centre of the bulk-mode band in Co/Ru multilayers versus the Ru layer thicknesses for the Co layer thickness of 20 Å. Oscillations with a period of 11.5 Å are well resolved for both curves. The observed frequency oscillations as a function of d_{Ru} are accompanied by oscillations with the same periodicity in the linewidths of the spin-wave modes. From the comparison of the experimental data with the results of the calculation based on an effective-medium model [112], the value of the interlayer coupling has been deduced. It is presented in the lower part of figure 26. The coupling is found to be of AF type in the limit of a very small Ru thickness. Similar results were also obtained for permalloy/Ru multilayers.

We should, nevertheless, note that magnetic behaviour of the multilayers with AF-type exchange at a low enough field, when the sample is not saturated, is very complicated. There are indications in the literature [113], that the ground state of such a multilayer may be more complex than the simple canted state. Moreover, an experimental investigation of Fe/Cr/Fe multilayers revealed for a certain applied field the existence of a spin-wave mode which cannot be attributed to the simple canted ground state [114].

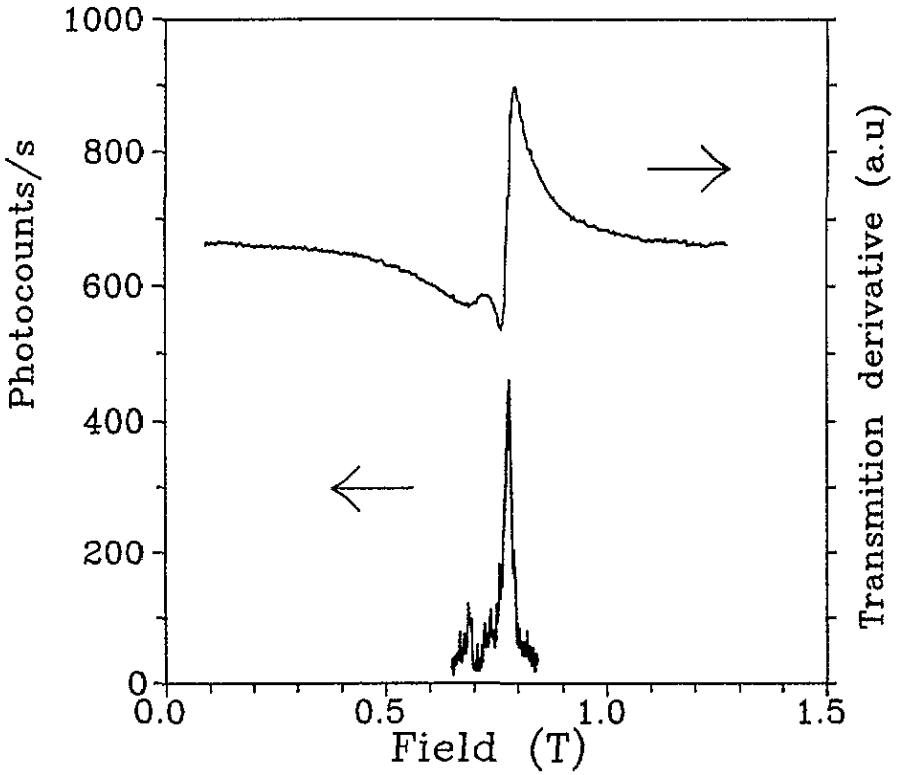

Figure 28. FMR lines in the Fe/Cr/Fe bilayer detected by microwave absorption and BLS (from [119]).

In conclusion of this section we notice that multilayers as well as single thin films can be used for the analysis of anisotropies. The magnitudes and spatial variation of magnetic anisotropies due to thickness variations of the Co layers were determined using BLS from collective spin-wave excitations in (111)-oriented and (100)-oriented epitaxial Co/Pt multilayers [115]. It was shown in [116] that the experimentally observed large uniaxial in-plane anisotropy in epitaxial (110)-oriented Co/Pt and Co/Pd multilayers is caused by magneto-elastic interaction. In the same work the lateral and layer-to-layer variations of anisotropies in Co/Pd and Co/Au multilayers were analysed by BLS experiments.

7. Non-thermal excited spin waves

Throughout the above we have discussed thermally excited spin waves. It was demonstrated that light scattering from thermally excited spin waves became a valuable tool for the investigation of the interlayer coupling in layered magnetic systems. Of particular importance is the possibility of studying a small area of the sample of the size of a focused laser beam. This gives us the opportunity to use wedge samples and, hence, to measure precisely the interlayer coupling depending on the thickness of specific layers. On the other hand, the method cannot be used either at low temperatures or for samples with small magneto-optic constants because of decreasing BLS intensity in both cases (see section 3). This disadvantage can be avoided by pumping spin waves by microwave power

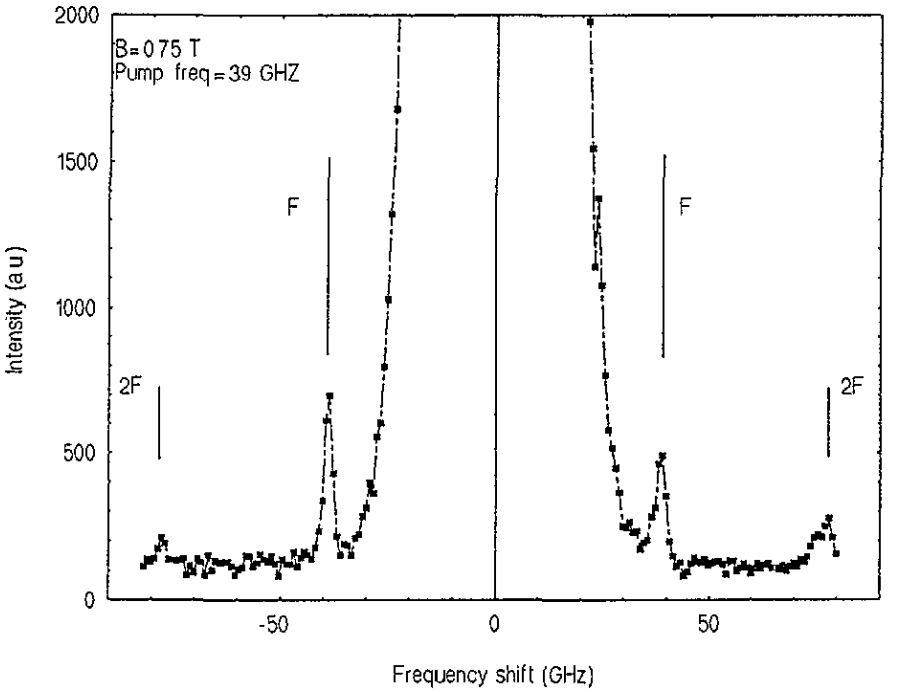

Figure 29. *BLS spectrum from pumped spin waves in the Fe/Cr/Fe bilayer. The pair of peaks* labelled 2F has a frequency shift that is twice that of the pumping frequency (from [119]).

as it is usually realized in the ferromagnetic resonance (FMR) technique. However, the FMR technique in the standard form can hardly be applied for systems with wedge-type interspacers where a local probe is needed for investigation.

The idea to combine BLS and FMR techniques was proposed and realized by Dillon *et al* [117] on bulk crystals of transparent $CrBr_3$. The beam passing through the crystal was analysed and BLS from bulk spin-wave modes with almost zero wavevector was detected (for details of BLS from pumped spin waves see the review [118]). Very recently a combined BLS–FMR technique was applied for investigation of an Fe/Cr/Fe layered system with a wedge-type Cr interlayer [119]. In this case a laser beam, reflected from the sample, was analysed by interferometer. This geometry corresponds to BLS from spin waves with $k_{\parallel} \simeq 0$. Since the experiments were performed at low temperature ($T = 2$ K), the light scattering from thermally excited spin waves was not detected. However, after excitation of FMR in the sample the BLS from spin waves, 'pumped' by microwave power, became observable.

A representative spectrum, taken from [119], is presented in figure 27. A pair of peaks with a frequency shift which is equal to the microwave frequency is clearly pronounced. The intensity of the shaded peak was used to detect the FMR curve. For continuous measurements of the peak intensity the technique described in subsection 4.2 was applied. The detected resonance line is presented in figure 28. For comparison the microwave absorption as a function of the applied field is also shown. Both curves manifest two resonances corresponding to the excitation of the in-phase and out-of-phase spin-wave modes in the bilayer. From the field positions of these resonances the value of the interlayer coupling can be derived.

A BLS spectrum with higher free spectral range of the interferometer is shown in figure 29. It clearly demonstrates the existence of the second pair of peaks with a frequency

shift that is twice the pumping frequency. So far it is not clear whether this is due to the creation of one spin wave with a doubled frequency by two microwave photons or due to the many-magnon BLS process, in which a pair of spin waves takes part.

A peculiar asymmetry in the intensity of the Stokes and anti-Stokes lines is distinctly seen in figure 27 and figure 29. This asymmetry does not change with a reversal of magnetization and rotation of the polarization of the incident light. Among the reasons known to cause the Stokes–anti-Stokes asymmetry (see section 3), only that connected with the small value of occupation numbers n_ω has the same features. However, this mechanism cannot explain the finding, because the estimation of n_ω made from the absolute value of BLS gives $n_\omega > 20$. This corresponds to a Stokes–anti-Stokes asymmetry of less than 5%. Thus, the origin of this asymmetry is still unknown.

Parametric pumping is also widely used for the excitation of spin waves in magnetic solids (see [118]). In this process a microwave photon creates two spin waves with antiparallel wavevectors and half frequencies. However, for the realization of parametric pumping the microwave power should exceed the threshold, which depends on the damping in the magnetic subsystem of the crystal. In metallic magnetic solids such damping is much higher than in insulators, therefore experiments on parametric pumping in metals need much more powerful microwave sources and will probably be the subject of future investigations.

Acknowledgments

The authors are grateful to P Grünberg for stimulating and helpful discussions. We are especially indebted to W Zinn for his interest in the work. One of the authors (ET) is pleased to thank the Alexander von Humboldt Foundation for support.

References

[1] Grunberg P and Metawe F 1977 *Phys. Rev. Lett.* **39** 1561
[2] Borovik-Romanov A S and Kreines N M 1982 *Phys. Rep.* **81** 351; 1988 *Spin Waves and Magnetic Excitations 1* ed A S Borovik-Romanov and S K Sinha (Amsterdam: Elsevier) p 81
[3] Patton C 1984 *Phys. Rep.* **103** 251
[4] Grünberg P 1985 *Prog. Surf. Sci.* **18** 1; 1989 *Light Scattering in Solids V: Superlattices and other Microstructures* ed M Cardona and G Güntherodt (Berlin: Springer) p 303
[5] Cottam M G and Lockwood D J 1986 *Light Scattering in Magnetic Solids* (New York: Wiley)
[6] Benson H and Mills D L 1969 *Phys. Rev.* B **18** 839
[7] Akhiezer A I, Bar'yaktar V G and Peletminskii S V 1969 *Spin Waves* (Amsterdam: North-Holland)
[8] Wolfram T and De Wames R E 1972 *Prog. Surf. Sci.* **2** 233
[9] Rado G T and Hicken R J 1989 *J. Appl. Phys.* **63** 3885
[10] Damon R W and Eschbach J R 1961 *J. Phys. Chem. Solids* **19** 308
[11] Kalinikos B A and Slavin A N 1986 *J. Phys. C: Solid State Phys.* **19** 7013
[12] Vayhinger K and Kronmüller H 1986 *J. Magn. Magn. Mater.* **62** 159
[13] Tsymbal E 1994 *J. Magn. Magn. Mater.* **130** 46
[14] Cochran J F and Dutcher J R 1988 *J. Appl. Phys.* **63** 3814
[15] De Wames R E and Wolfram T 1970 *J. Appl. Phys.* **41** 987
[16] Rado G T and Weertman J R 1959 *J. Phys. Chem. Solids* **11** 315
[17] Mills D L and Maradudin A A 1967 *J. Phys. Chem. Solids* **28** 1855
[18] Puszkarski H 1979 *Prog. Surf. Sci.* **9** 191
[19] Moul R C and Cottam M G 1983 *J. Phys. C: Solid State Phys.* **16** 1307
[20] Grünberg P, Cottam M G, Vach W, Mayr C and Camley R E 1982 *J. Appl. Phys.* **53** 2078
[21] Stamps R L and Hillebrands B 1991 *Phys. Rev.* B **44** 12417
[22] Grünberg P 1980 *J. Appl. Phys.* **51** 4338

[23] Grünberg P 1981 *J. Appl. Phys.* **52** 6824
[24] Camley R E and Maradudin A A 1982 *Solid State Commun.* **41** 585
[25] Vayhinger K and Kronmüller H 1988 *J. Magn. Magn. Mater* **72** 307
[26] Barnaś J and Grünberg P 1989 *J. Magn. Magn. Mater.* **82** 186
[27] Vohl M, Barnaś J and Grünberg P 1989 *Phys. Rev.* B **39** 12003
[28] Hillebrands B 1990 *Phys. Rev.* B **41** 530
[29] Hoffmann F 1970 *Phys. Status Solidi* **47** 807
[30] Camley R E, Rahman T and Mills D L 1983 *Phys. Rev.* B **27** 261
[31] Grünberg P and Mika K 1983 *Phys. Rev.* B **27** 2955
[32] Mika K and Grünberg P 1985 *Phys. Rev.* B **31** 4465
[33] Emtage P R and Daniel M R 1984 *Phys. Rev.* B **29** 212
[34] Rupp G, Wettling W and Jantz W 1987 *Appl. Phys.* A **42** 45
[35] Hinchey L L and Mills D L 1986 *Phys. Rev.* B **33** 3329
[36] Barnaś J 1988 *J. Phys. C: Solid State Phys.* **21** 1021
[37] Hillebrands B 1988 *Phys. Rev.* B **37** 9885
[38] Stamps R L, Camley R E, Hillebrands B and Güntherodt G 1993 *Phys. Rev.* B **47** 5072
[39] Shen Y R and Bloembergen N 1966 *Phys. Rev.* **143** 372
[40] Fleury P A and Loudon R 1968 *Phys. Rev.* **166** 514
[41] Moriya T 1967 *J. Phys. Soc. Japan* **23** 163
[42] Le Gall H and Jamet J P 1971 *Phys. Status Solidi* **46** 467
[43] Wettling W, Cottam M G and Sandercock J R 1975 *J. Phys. C: Solid State Phys.* **8** 211
[44] Cottam M G 1976 *J. Phys. C: Solid State Phys.* **9** 2137
[45] Camley R E, Rahman T S and Mills D L 1981 *Phys. Rev.* B **23** 1226
[46] Camley R E, Grünberg P and Mayr C M 1982 *Phys. Rev.* B **26** 2609
[47] Cochran J F and Dutcher J R 1988 *J. Appl. Phys.* **63** 3814
[48] Rojdestvenski I V, Cottam M G and Slavin A N 1993 *Phys. Rev.* B **48** 12768
[49] Landau L D and Lifshitz E M 1960 *Electrodynamics of Continuous Media* (Oxford: Pergamon)
[50] Camley R E and Mills D L 1978 *Phys. Rev.* B **18** 4821
[51] Demokritov S O, Kreines N M and Kudinov V I 1987 *Zh. Eksp. Teor. Fiz.* **92** 689 (Engl. Transl. 1987 *Sov. Phys.–JETP* **65** 389)
[52] Grünberg P and Metawe F 1977 *Phys. Rev. Lett.* **39** 1561
[53] Gradmann U 1993 *Handbook of Magnetic Materials* vol 7, ed K H J Buschow (Amsterdam: Elsevier)
[54] Bauer E 1982 *Appl. Surf. Sci.* **11/12** 429
[55] Bauer E 1958 *Z. Kristallogr.* **110** 37
[56] Prinz G A 1985 *Phys. Rev. Lett.* **54** 1051
[57] Krams P, Hillebrands B, Güntherodt G and Oepen H P 1994 *Phys. Rev.*B **49** 3633
[58] Hillebrands B, Baumgart P and Güntherodt G 1989 *Appl. Phys.* A **49** 589
[59] Heinrich B, Urquhart K B, Dutcher J R, Purcell S T, Cochran J F, Arrott A S, Steigerwald D A and Egelhoff W F Jr 1988 *J. Appl. Phys.* **63** 3863
[60] Steigerwald D A and Egelhoff W F Jr 1987 *Surf. Sci.* **192** L887
[61] Grünberg P, Demokritov S, Fuss A, Schreiber R, Wolf J A and Purcell S T 1992 *J. Magn. Magn. Mater.* **104-107** 1734
[62] Heinrich B, Form M, Cochran J F, Liao L X, Celinski Z, Schneider C M and Myrtle K 1993 *Mater. Res. Soc. Symp. Proc.* vol 313, ed B T Jonker *et al* (Pittsburgh, PA: Materials Research Society) p 119
[63] Unguris J, Celotta R and Pierce D T 1991 *Phys. Rev. Lett.* **67** 140
[64] Unguris J, Celotta R and Pierce D T 1993 *J. Magn. Magn. Mater.* **127** 205
[65] Parkin S S P 1991 *Phys. Rev. Lett.* **67** 3598
[66] Sandercock J R 1975 *RCA Rev.* **36** 89
[67] Sandercock J R 1982 *Light Scattering in Solids III* ed M Cardona and G Güntherodt (Heidelberg: Springer)
[68] May W, Kiefte H, Clouter M J and Stegeman G 1978 *Appl.Opt.* **17** 1603
[69] Rowell N L, Lockwood D J and Grant P 1981 *J. Raman Spectrosc.* **10** 119
[70] Borovik-Romanov A S, Demokritov S O, Kreines N M and Kudinov V I 1985 *Zh. Eksp. Teor. Fiz.* **88** 1348 (Engl. Transl. 1985 *Sov. Phys.–JETP* **61** 801)
[71] Demokritov S, Wolf J A and Grünberg P 1991 *Europhys.Lett* **15** 881
[72] For a review see: Pokrovskii V L and Uimin G V 1990 *Magnetic Properties of Layered Transition Metal Compounds* ed L J de Jongh (Deventer: Kluwer)
[73] Mermin N D and Wagner H 1966 *Phys. Rev. Lett.* **17** 1133
[74] Gradmann U 1984 *Phys. Rev. Lett.* **52** 771
[75] Patashinskii A Z and Pokrovskii V L 1979 *Fluctuational Theory of Phase Transitions* (Oxford: Pergamon)

[76] Pokrovskii V L and Feigelmann M V 1977 *Zh. Eksp. Teor. Fiz.* **72** 557 (Engl. Transl. 1977 *Sov. Phys.–JETP* **45** 291)
[77] *Kerkmann D, Wolf J A, Pescia D, Woike Th and Grünberg P 1989 Solid State Commun.* **72** 963
[78] Demokritov S O, Kreines N M, Kudinov V I and Petrov S V 1989 *Zh. Eksp. Teor. Fiz.* **95** 2211 (Engl. Transl. 1989 *Sov. Phys.–JETP* **68** 1277)
[79] den Broeder F J A, Kuiper D, Donkersloot H C and Hoving W 1989 *Appl. Phys.* A **49** 507
[80] *Hillebrands B, Baumgart P and Güntherodt G 1989 Appl. Phys. A* **59** *589*
[81] Cochran J F, Heinrich B, Arrott A S, Urquhart K B, Dutcher J R and Purcell S T 1989 *J. Physique Coll. Suppl.* 12 **49** C8 1671
[82] Dutcher J R, Heinrich B, Cochran J F, Steigerwald D A and Egelhoff W F Jr 1989 *J. Appl. Phys.* **63** 3464
[83] Dutcher J R, Cochran J F, Jacob I and Egelhoff W F Jr 1989 *Phys. Rev.* B **39** 10430
[84] Dutcher J R, Cochran J F, Heinrich B and Arrott A S 1988 *J. Appl. Phys.* **63** 6095
[85] Urquhart K B, Heinrich B, Cochran J F, Arrott A S and Myrtle K 1988 *J. Appl. Phys.* **64** 5334
[86] Gay J G and Richter R 1986 *Phys. Rev. Lett.* **56** 2728
[87] Murayama A, Miyamura M, Nishiyama K, Miyata K and Oka Y 1991 *J. Appl. Phys.* **69** 5661
[88] Murayama A, Miyamura M, Ishikawa S and Oka Y 1990 *J. Appl. Phys.* **67** 410
[89] Yoshihara A, Haneda Y, Shimada Y and Fujimura T 1989 *J. Appl. Phys.* **65** 4968
[90] Grünberg P, Schreiber R, Pang Y, Brodsky M B and Sowers H 1986 *Phys. Rev. Lett.* **57** 2442
[91] Baibich M N, Broto J M, Fert A, Nguyen Van Day F, Petroff F, Etienne P, Creuzet G, Friederich A and Chazelas J 1988 *Phys. Rev. Lett.* **61** 2472
[92] Binash G, Grünberg P, Saurenbach F and Zinn W 1989 *Phys. Rev.* B **39** 482
[93] Heinrich B, Purcell S T, Dutcher J R, Urquhart K B, Cochran J F and Arrott A S 1988 *Phys. Rev.* B **38** 12 879
[94] Demokritov S, Tsymbal E, Grünberg P, Zinn W and Schuller I K 1994 *Phys. Rev.* B **49** 720
[95] Rudermann M A and Kittel C 1956 *Phys. Rev.* **87** 440
Kasuya T 1956 *Prog. Theor. Phys.* **16** 45
Yosida K 1957 Phys. Rev. **106** 893
[96] Grünberg P, Barnas J, Saurenbach F, Fuss A, Wolf J A and Vohl M 1991 *J. Magn. Magn. Mater.* **93** 58
[97] Fuss A, Demokritov S, Grünberg P and Zinn W 1992 *J. Magn. Magn. Mater.* **103** L221
[98] Cochran J F, Rudd J, Muir W B, Heinrich B and Celinski Z 1990 *Phys. Rev.* B **42** 508
[99] For a recent review of the subject see *1993 Proc. Int. Symp. on Metallic Multilayers (Kyoto, 1993); J. Magn. Magn. Mater.* **126**
[100] Parkin S S P, More N and Roche K P 1990 *Phys. Rev. Lett.* **64** 2304
[101] Grünberg P, Demokritov S, Fuss A, Vohl M and Wolf J A 1991 *J. Appl. Phys.* **69** 4789
[102] Ruhrig M, Schafer R, Hubert A, Mosler R, Wolf J A, Demokritov S and Grünberg P 1991 *Phys. Status Solidi* a **125** 635
[103] Demokritov S, Wolf J A, Grünberg P and Zinn W 1991 *Mater. Res. Soc. Symp. Proc.* vol 231, ed S S P Parkin *et al* (Pittsburgh, PA: Materials Research Society) p 133
[104] Wang J Y, Levy P M and Frey-J L 1990 *Phys. Rev. Lett.* **65** 2732
[105] *Mathon J, Edwards D M, Muniz R B and Phan M S 1992 J. Magn. Magn. Mater.* **104–107** 1721
[106] Grünberg P, Demokritov S, Fuss A, Schreiber R, Wolf J A and Purcell S T 1992 *J. Magn. Magn. Mater.* **104-107** 1734
[107] Kabos P, Patton C E, Dima M O, Church D B, Stamps R L and Camley R E 1994 *J. Appl. Phys.* **75** 3553
[108] Kueny A, Khan M R, Shuller I K and Grimsditch M 1984 *Phys. Rev.* B **29** 2879
[109] Hillebrands B, Harzer J V, Güntherodt G, England C D and Falco C M 1990 *Phys. Rev.* B **42** 6839
[110] Fassbender J, Nörtermann F, Stamps R L, Camley R E, Hillebrands B, Güntherodt G and Parkin S S P 1992 *Phys. Rev.* B **46** 5810
[111] Fassbender J, Nörtermann F, Stamps R L, Camley R E, Hillebrands B, Güntherodt G and Parkin S S P 1993 *J. Magn. Magn. Mater.* **121** 270
[112] Almeida N S and Mills D L 1988 *Phys. Rev.* B **38** 6698
[113] Nörtemann F C, Stamps R L, Carrica A S and Camley R E *Phys. Rev.*B **46** 10 847
[114] Yoshihara A, Takanashi K, Obi Y and Fujimori H 1993 *J. Magn. Magn. Mater.* **126** 333
[115] Harzer J V, Hillebrands B, Stamps R L, Güntherodt G, Weller D, Lee Ch, Farrow R F C and Marinero E E 1992 *J. Magn. Magn. Mater.* **104–107** 1863
[116] Hillebrands B, Harzer J V, Güntherodt G and Dutcher J R *J. Japan Magn. Soc.* at press
[117] Dillon J F Jr, Kamimura H and Remeika J P 1963 *J. Appl. Phys.* **34** 1240
[118] Borovik-Romanov A S and Kreines N M 1982 *Phys. Rep.* **81** 351
[119] Demokritov S O 1993 *J. Magn. Magn. Mater.* **126** 291